NASA/TM-2004-213267

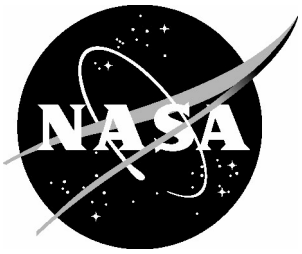

Effect of Blowing on Boundary Layer of Scarf Inlet

Carl H. Gerhold and Lorenzo R. Clark
Langley Research Center, Hampton, Virginia

December 2004

The NASA STI Program Office . . . in Profile

Since its founding, NASA has been dedicated to the advancement of aeronautics and space science. The NASA Scientific and Technical Information (STI) Program Office plays a key part in helping NASA maintain this important role.

The NASA STI Program Office is operated by Langley Research Center, the lead center for NASA's scientific and technical information. The NASA STI Program Office provides access to the NASA STI Database, the largest collection of aeronautical and space science STI in the world. The Program Office is also NASA's institutional mechanism for disseminating the results of its research and development activities. These results are published by NASA in the NASA STI Report Series, which includes the following report types:

- TECHNICAL PUBLICATION. Reports of completed research or a major significant phase of research that present the results of NASA programs and include extensive data or theoretical analysis. Includes compilations of significant scientific and technical data and information deemed to be of continuing reference value. NASA counterpart of peer-reviewed formal professional papers, but having less stringent limitations on manuscript length and extent of graphic presentations.

- TECHNICAL MEMORANDUM. Scientific and technical findings that are preliminary or of specialized interest, e.g., quick release reports, working papers, and bibliographies that contain minimal annotation. Does not contain extensive analysis.

- CONTRACTOR REPORT. Scientific and technical findings by NASA-sponsored contractors and grantees.

- CONFERENCE PUBLICATION. Collected papers from scientific and technical conferences, symposia, seminars, or other meetings sponsored or co-sponsored by NASA.

- SPECIAL PUBLICATION. Scientific, technical, or historical information from NASA programs, projects, and missions, often concerned with subjects having substantial public interest.

- TECHNICAL TRANSLATION. English-language translations of foreign scientific and technical material pertinent to NASA's mission.

Specialized services that complement the STI Program Office's diverse offerings include creating custom thesauri, building customized databases, organizing and publishing research results ... even providing videos.

For more information about the NASA STI Program Office, see the following:

- Access the NASA STI Program Home Page at ***http://www.sti.nasa.gov***

- E-mail your question via the Internet to help@sti.nasa.gov

- Fax your question to the NASA STI Help Desk at (301) 621-0134

- Phone the NASA STI Help Desk at (301) 621-0390

- Write to:
  NASA STI Help Desk
  NASA Center for AeroSpace Information
  7121 Standard Drive
  Hanover, MD 21076-1320

NASA/TM-2004-213267

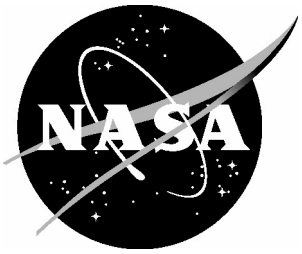

Effect of Blowing on Boundary Layer of Scarf Inlet

Carl H. Gerhold and Lorenzo R. Clark
Langley Research Center, Hampton, Virginia

National Aeronautics and
Space Administration

Langley Research Center
Hampton, Virginia 23681-2199

December 2004

Acknowledgments

The authors wish to acknowledge the assistance of Ms. Beverly Anderson of the Aeroacoustics and Hypersonic Propulsion Support Section, AAAC, who led the team of technicians setting up the experiment. The efforts of Mr. Phil Grauberger, Wyle Laboratories, who oversaw installation and calibration of the data acquisition system as well as the acquisition of acoustic data; and Mr. Lawrence Becker, Lockheed Martin Services, who oversaw data reduction and plot preparation are also gratefully acknowledged.

Available from:

NASA Center for AeroSpace Information (CASI)
7121 Standard Drive
Hanover, MD 21076-1320
(301) 621-0390

National Technical Information Service (NTIS)
5285 Port Royal Road
Springfield, VA 22161-2171
(703) 605-6000

Abstract

When aircraft operate in stationary or low speed conditions, airflow into the engine accelerates around the inlet lip and pockets of turbulence that cause noise and vibration can be ingested. This problem has been encountered with engines equipped with the scarf inlet, both in full scale and in model tests, where the noise produced during the static test makes it difficult to assess the noise reduction performance of the scarf inlet. NASA Langley researchers have implemented boundary layer control in an attempt to reduce the influence of the flow nonuniformity in a 12-in. diameter model of a high bypass fan engine mounted in an anechoic chamber. Static pressures and boundary layer profiles were measured in the inlet and far field acoustic measurements were made to assess the effectiveness of the blowing treatment. The blowing system was found to lack the authority to overcome the inlet distortions. Methods to improve the implementation of boundary layer control to reduce inlet distortion are discussed.

Introduction

The scarf inlet, shown in figure 1(a), is one in which the inlet lip protrudes more at the lower lip (keel) than at the upper lip (crown). This design has the potential to reduce inlet-radiated fan noise by redirecting a part of the acoustic energy up and away from observers on the ground. A computational analysis of the scarf inlet concept (ref. 1) demonstrated that the scarf inlet may also have a reduced tendency to ingest foreign objects from the ground during takeoff and landing runs and that it can maintain attached internal flow at higher angle of attack than axisymmetric inlets. The analysis included general design guidelines for scarf inlets based on the parameters of inlet internal lip thickness, axial extent of the keel extension, and circumferential extent of the transition from keel to crown. A critical parameter in reducing the internal flow separation from the inlet upper lip is the area contraction ratio, which is expressed as the square of the ratio of the diameter at the inlet leading edge (highlight) to the diameter of the throat (fig. 1(a)). As this ratio increases, larger amounts of lower lip extension can be accommodated without internal flow separation. As the forward speed of the aircraft increases, the dependence of internal flow separation on area contraction ratio decreases, and the critical parameter becomes the scarf angle. Thus, a relatively larger contraction ratio is required to control internal flow separation at static conditions than that required for cruise. Increasing the area contraction ratio increases the thickness of the inlet wall, which adds weight and drag (ref. 1).

Several prototype scarf inlets have been fabricated for model and for full scale engine testing. The scarf inlet discussed in this paper was tested previously in forward flow in the 14- by 22-Foot Subsonic Tunnel at Langley Research Center (ref. 2). The experiment showed that the model engine equipped with a scarf inlet radiated less noise into the forward sector below the inlet than did the model when it was equipped with a symmetric inlet. The difference is fairly broadband, extending over one-third octave bands from 2000 to 15 000 Hz. Although the difference is on the order of 0.5 dB (OASPL), the indication is that the scarf inlet reflects a portion of the acoustic energy away from the ground. One conclusion from the study is that a more aggressive scarf design may provide more noise reduction. Because of safety issues and the high expense of flight testing, in situ validation of noise control technologies, such as the scarf inlet, is often done on a static test stand. A common problem that exists in static engine noise tests is that the engine is pulling air in from a quiescent medium and the turbulence that arises from the separated

flow at the inlet lip is ingested, therefore causing spurious noise to be generated, particularly at the blade-passage frequency. The turbulence intensity is generally less once the aircraft is moving; therefore, the turbulence-generated noise is reduced. In order to simulate forward flight during static testing, an inflow control device is used. The inflow control device is a large, hollow, removable sphere that can be rolled into place surrounding the inlet. It is fabricated from honeycomb material with cells oriented along lines of potential flow into the inlet. The effectiveness of the inflow control device has been demonstrated for symmetric inlet designs (ref. 3). Despite the presence of the inflow control device, unexpectedly high blade-passage frequency tones have been measured during acoustic tests on engines equipped with the scarf inlet, in full scale and model tests alike. A tone is generated intermittently at the blade-passage frequency, which indicates intermittent ingestion of turbulence. Low frequency noise occurs at high fan speeds, indicating onset of rotor stall. While the expectation is that the inflow distortion causing these tones will be decreased when the aircraft is in forward flight, the noise produced during the static test makes it difficult to validate those noise reduction results representative of the full scale inlet in flight. In addition, the noise and vibration induced by the inlet at low forward speed, such as during ground operation, could shorten the service life of the engine. Researchers at Langley Research Center have investigated the cause of the inflow distortion and the development of a control system using boundary layer control to reduce the influence of the flow nonuniformity.

A computational study of the scarf inlet, verified by experiment, located the inlet separation on the half of the inlet surrounding the crown. The analytical study further recommended boundary layer control in the vicinity of the highlight. One such control feature, boundary layer suction, has been implemented on the model inlet, evaluated experimentally, and reported in the open literature (ref. 4). Another recommended modification is blowing into the boundary layer. This modification was implemented and evaluated in terms of its effectiveness both aerodynamically and acoustically and is the subject of this report.

Acronyms

OASPL overall sound pressure level re 20×10^{-6} Pa

ADP Advanced Ducted Propeller

BPF blade-passage frequency

SPL sound pressure level re 20×10^{-6} Pa

Methods and Equipment

Experiment Facility and Model Fan

The control system was developed on a 12-in. diameter model of a high bypass fan engine mounted in an anechoic chamber. The 12-in. Advanced Ducted Propeller (ADP) Demonstrator has 16 wide-chord rotor blades with a hub-to-tip ratio of 0.445. A row of 40 stator vanes is located 2 blade chords downstream of the rotors. This combination of blades and vanes is used in order that the lowest mode of rotor/stator interaction noise is evanescent (ref. 5) and no tone at the blade passage frequency is expected to radiate. Figure 1(b) shows the 12-in. ADP Demonstrator with the scarf inlet in place. A 4-stage turbine driven by compressed air powers the model. The model is based on high bypass ratio, high subsonic tip speed engines. The rotor tip speed at 100 percent is subsonic at 905 ft/s. The blade angle setting is fixed at the takeoff condition and the fan pressure ratio is 1.27 at 100-percent speed (ref. 6). The model scarf inlet is equipped with two rows of static pressure taps extending from the inlet highlight to the rotor plane, as

indicated in figure 1(b). One row is located at the crown of the scarf inlet, where the axial distance from the highlight to the rotor plane is minimum, and the other row is at the midpoint between the crown and the keel. Two boundary layer rakes are mounted near the rotor plane of the inlet, one at the keel and the other at the midpoint opposite the static array. These boundary layer rakes can be seen in figure 1(b) although they are removed during acoustic tests. Pressure data are collected on a Pressure Systems Incorporated model ESP 8400 multichannel pressure data acquisition system. In a typical data acquisition, all data channels are sampled 32 times and the average computed. Thirty-two samples of the average pressures are written to a file so that an average steady state pressure, as well as the standard deviation, can be evaluated for each channel. The entire process of data acquisition of 1024 points per channel takes approximately 8 s in real time.

All acoustic and aerodynamic testing of the model during this test were performed in the Anechoic Noise Research Facility at Langley Research Center in Hampton, Virginia, although reference is made to tests performed previously on the model in the Center's 14- by 22-Foot Subsonic Tunnel. The anechoic chamber is a static facility; however, it is ventilated such that adequate flow is available to the fan to simulate an outdoor static test stand. The chamber's dimensions are 27.5 ft × 27.5 ft × 24 ft inside the acoustic wedges. The acoustic treatment is designed to absorb 99 percent of incident sound energy above 100 Hz.

Acoustic measurements are made using a 6-ft diameter hoop array on which 18 microphones are mounted on equal spacing of 20°. The hoop can be rotated such that sound measurements are taken in the azimuth with resolution of 4°, and the array can be translated to permit measurements on polar angles from 15° from the engine axis to 75° (ref. 7). The microphones are Bruel & Kjaer model 4135, 0.25-in. diameter laboratory quality condenser transducers. The microphone signals are conditioned first using Bruel & Kjaer model 2811 multiplexers, then Precision Filters filter/amplifiers. The filters are set at 200 Hz high pass and 50 kHz low pass. The data are recorded using a NEFF Instruments 495 high-speed multichannel data acquisition system. In a typical data collection, 19 channels (18 microphones plus engine tachometer) of data are recorded for 4 s at a rate of 100 000 samples/s. The microphone system is calibrated daily using a Bruel & Kjaer model 4226 multifunction acoustic calibrator.

Modifications to Model Fan

Flow into the scarf inlet is distorted because of the nonsymmetry of the inlet shape. The inflow distortion is most severe when the engine is at rest because the engine is pulling air from the quiescent medium. The inflow distortion results in a circumferentially nonuniform boundary layer near the rotor. This boundary layer is relatively thin in the region of the keel and thickens toward the crown. The flow in the boundary layer is reversed in the crown half of the inlet. The flow reversal begins in the area of the midpoint between the crown and the keel and becomes more severe as the crown is approached. Because the flow is accelerated more rapidly around the highlight in the region of the crown, the inflow speed is higher near the crown than it is near the keel. It is expected that the inflow distortion will decrease with increasing forward speed. This reduced inflow distortion is evidenced by a tendency toward increasing circumferential uniformity of the boundary layer profile, as well as uniform flow speed into the rotor.

A previous attempt was made to reduce the inflow distortion when the engine is at rest on a test stand by introducing suction just downstream of the highlight (ref. 4). Eighty suction tubes were mounted on the inlet spanning ±90° from the engine crown. The tubes were mounted on the outside of the inlet and bored through to the inside surface. The suction was found to reduce the variability of engine speed and to improve stall margin; however, the suction system did not meet the design goal of producing the inflow uniformity associated with forward flight. It was also found that the tubes mounted on the outside of the

inlet disturbed the reverse flow near the highlight to the extent that it was difficult to determine the impact of suction on engine performance apart from the impact of the presence of the tubes themselves.

The second phase of the project involves the use of blowing to reduce inflow distortion. Air is introduced on the exterior surface of the inlet near the highlight in a range spanning ±90° from the crown. This auxiliary flow is intended to counteract the reversed flow that occurs in the region of the crown.

The air is injected from 80 tubes that are mounted parallel to the fan axis and that discharge near the inlet highlight. The blowing tube insertion points are indicated in the scarf inlet sketch (fig. 1(a)). Three locations of discharge were evaluated: 0.125 in. downstream of the inlet highlight, 0.500 in. downstream, and 0.875 in. downstream. The 0.125-in. location is chosen to put the point of air injection as close as possible to the highlight. The 0.875-in. dimension corresponds to the location of the inlet throat and was the penetration point of the suction tubes in the companion suction experiment (ref. 4). The 0.5-in. location is selected as the midpoint between the two extremes. Figure 2 shows the scarf inlet with the tube array mounted in the 0.125-in. location. The tubes are each 0.060-in. OD and 0.040-in. ID. Airflow to each of the 80 blowing ports can be controlled individually because air is supplied to each port via a proportional control valve. Two air injection configurations are reported here. The first is one in which all valves are open the same amount so that flow into the inlet is uniform from all ports; the other is one in which the valves are opened proportionally around the circumference. In this latter configuration, designated "shaped blowing" in subsequent figures, flow from ports near the crown is maximum and it decreases to zero toward the midpoints between the crown and the keel. The supply pressure is approximately 125 psi and it was found that the maximum flow rate with all valves fully open is 14.5 ft^3/min. This flow rate corresponds to ≈0.10 percent of the flow rate through the bypass duct of the ADP Demonstrator. The maximum flow rate is limited by the choked flow in the 0.040-in. tubes.

The engine is operated at four speeds: 70, 80, 90, and 100 percent of maximum speed, where 100 percent is 17500 rpm. Pressure measurements are taken at each speed setting with the air supply turned off, with all the valves open uniformly, and with the shaped blowing configuration. The boundary layer rakes are removed and acoustic surveys of inlet-radiated noise are made at the same four speed settings with the air supply turned off, the valves all open uniformly, and the shaped blowing configuration. Because the test's purpose is to achieve flight conditions with the air injection system, the inflow control device is not installed during these runs of the ADP Demonstrator. However, a separate acoustic data survey was made with the air injection tubes removed and the inflow control device in place.

Results

Boundary Layer at Midpoint Between Keel and Crown

The boundary layer profile at this location is strongly influenced by the inflow distortion. Figures 3 through 5 show the boundary layer profile at the midpoint between the crown and the keel for engine speeds at 70, 80, and 100 percent. The curve identified as "unmodified" is based on data that were measured before any modifications to the inlet were made. Because it is reasonable to expect that boundary layer thickness can be related to the shapes of these curves, the shape desired is one in which the profile knee is close to zero radial location. The curve shifts to the right, indicating a thicker boundary layer, as the speed is increased. This shift was accompanied by an increasing inability to hold speed constant in the ADP Demonstrator at higher speeds and a tendency of the rotor to go into stall. Thus, the desired outcome of the air injection is to shift the pressure profile curves toward the left, indicating reduced boundary layer thickness.

The data shown in figures 3 through 5 are for the tubes located 0.125 in. downstream of the highlight. The boundary layer profiles shift to the left dramatically at all speeds when the blowing tubes are in place, even with the blowing off. Such a shift is indicative of boundary layer thinning. Turning blowing on uniformly to all tubes has a small impact on the boundary layer profile in comparison to the blowing off case. Figures 6 and 7 show the effect of the shaped blowing at two engine speeds, 70 and 100 percent. Shaping the flow into the inlet boundary layer results in a small but beneficial shift of the boundary layer profile to the left at 70-percent speed (fig. 6), although no difference is seen between the blowing off and blowing on cases at 100-percent speed (fig. 7).

Figures 8 and 9 show the effect of location of the tubes at 0.875 in. downstream of the highlight, the farthest downstream location, when the ADP Demonstrator is operated at 70-percent speed. The boundary layer profile is shifted farthest to the left when the tubes are in place and blowing is turned off. When uniform blowing is turned on, the curves actually shift to the right, indicating a thicker boundary layer and degraded performance, as is seen in figure 8. The impact of shaping the flow is quite small in comparison to no flow (fig. 9). Figures 10 and 11 are the boundary layer profiles measured with the tubes at 0.875 in. downstream and the ADP Demonstrator operated at 100 percent. The conclusions are similar to those made for the 70-percent speed: the presence of the tubes has the greatest effect, uniform blowing actually shifts the profiles to the right, and shaped blowing does not change the profiles.

Figures 12 through 15 show the effect of blowing tube placement on the boundary layer profile at the midpoint for speeds at 70, 80, 90, and 100 percent, respectively. The figures show that, even with blowing turned off, the profiles shift toward the left uniformly as the tubes are moved forward toward the highlight.

Boundary Layer at Keel

Because the control is located nearer the inlet crown, it is not expected that the boundary layer at the keel will be influenced by disturbances to the boundary layer in the crown's vicinity. This is borne out in figures 16 through 19 for speeds of 70 through 100 percent. The presence of the blowing tubes has negligible effect on the boundary layer profile on the keel except at the maximum speed (fig. 19). This figure shows a slight shift of the profile to the left, and the shift is identical for all three tube placements. Figure 20 shows the effect of activating blowing on the boundary layer profile at the keel at 100-percent speed. This curve shows that blowing has no effect on the boundary layer profile at the keel, and it is typical of all results noted at other speeds and tube locations.

Boundary Layer Thickness and Inflow Mach Number Calculations

Boundary layer thickness is calculated by estimating from boundary layer profiles the point at which the pressure is 99 percent of the free-stream pressure. These calculated values are summarized in table 1 on the keel and table 2 at the midpoint between the keel and the crown. In each table the boundary layer thickness is shown at each engine speed for each of the air injection tube locations without air injection and with air injection uniform and shaped. The calculated boundary layer thickness based on data collected during runs with the 12-in. ADP Demonstrator installed in the 14- by 22-Foot Subsonic Tunnel is also shown (ref. 2). Those data were collected with the tunnel speed at Mach 0.15. The calculated thickness based on measurements with the 12-in. ADP Demonstrator installed in the Anechoic Noise Research Facility and operated before any modifications were made to the inlet is shown under the column heading "unmodified."

Comparison of the boundary layer thickness at the keel (table 1) and at the midpoint (table 2) from the wind tunnel tests with wind on at Mach 0.15 (last column) shows that the boundary layer thickness at the keel is 0.027 in. greater than it is at the midpoint at 70-percent fan speed, is the same at 90-percent speed, is 0.009 in. greater at 100-percent fan speed, and the boundary layer thickness is on the order of 0.10 in. or less. The next column to the left shows that when the wind is turned off and the 12-in. ADP Demonstrator is run, the boundary layer thickness is never less than 0.125 in. and exceeds 0.500 in. at 100-percent speed. The boundary layer thickness varies significantly between the keel and the midpoint. The relatively smaller variation of boundary layer thickness at the two points in the inlet in the presence of external flow is not proof, but it is suggestive of circumferential uniformity of the boundary layer in forward flight. This is the expected result of forward flight with the added expectation that uniform inflow reduces the inflow distortion that generates noise at blade-passage frequency (BPF) in the inlet. The relatively larger variation of boundary layer thickness with the inlet in the quiescent environment suggests a greater inflow nonuniformity and subsequent noise production.

Blowing air into the external boundary layer surrounding the inlet generally has very little effect on the boundary layer at the keel, as is shown in table 1. The results are similar whether air is on or there is no blowing. This result is expected because the air injection occurs on the crown of the inlet. There also does not appear to be any clear difference associated with location of the injection tubes relative to the highlight. Except at the highest fan speed, the boundary layer thickness on the keel is the same before and after modification of the inlet.

The effect of air injection is seen at the midpoint between the keel and the crown (see table 2). The calculations show that the closer to the highlight the air injection ports are installed, the thinner is the boundary layer. When the air injection ports are installed at 0.125 in. from the highlight, the shaped blowing, which concentrates air in the region of the crown, produces a thinner boundary layer than does uniform blowing. Generally, however, the results with blowing on are not significantly different from those with blowing off. This suggests that the greatest part of the beneficial effect of the boundary layer control system is due to the disturbance caused by the presence of the air injection tubes themselves.

The inflow Mach numbers are calculated at the throat based on the static pressure measurements from taps on the inlet inner surface. These static taps are located at the crown of the inlet and at the midpoint between the crown and the keel. The resultant calculations are summarized in tables 3 and 4. When the 12-in. ADP Demonstrator is operated with external flow of Mach 0.15, the circumferential variation in inflow Mach number between the two measurement points is relatively small, as expected. The two inflow Mach numbers are different by 8 to 11 percent over the range of operating speeds. In contrast, when the 12-in. ADP Demonstrator is run in the quiescent atmosphere, the difference of inflow Mach number is on the order of 40 percent between the two measurement locations. In both cases, the rate of change of inflow Mach number with engine operating speed is similar with the Mach number higher in the quiescent atmosphere. The installation of the air injection tubes does not seem to have any effect to reduce either the overall inflow Mach number or the variability of the Mach number between the two measurement locations.

Acoustic Survey

Figure 21 shows the 12-in. ADP Demonstrator in the anechoic chamber configured for acoustic testing. An acoustically treated baffle that eliminates flanking of duct discharge-radiated noise into the inlet region surrounds the inlet. The microphone hoop array is also shown in the photograph. Acoustic surveys were taken as described previously. The data were digitally fast Fourier transformed in order to produce spectra. The BPF tone and its 1st harmonic were extracted from the data and plotted to produce contours

of sound pressure level. The plots show sound pressure level (SPL re 20×10^{-6} Pa) on a cylinder encompassing azimuthal angles extending from 0° (directly below the inlet) to 180° (directly above the inlet) on the port side and to −180° on the starboard side. Axial locations are from 1.09 fan diameter upstream of the stacking point of the rotor to 11.2 fan diameter upstream. This range of axial locations covers the polar angle range from 70° to 15° from the axis of the fan.

Figures 22 through 24 are the contours of inlet-radiated SPL at BPF for the scarf inlet with the air injection tubes at 0.125 in. from the highlight for engine operating at 70-percent speed. Figure 22 is for blowing turned off. The effectiveness of the scarf inlet to redirect the inlet-radiated sound is seen. The sound level directly below the inlet is in the range of 107 dB; directly above the inlet the sound level is in the range of 112 dB. The zone of relative quiet in the shadow of the scarf inlet is small. A strong lobe of magnitude 113 dB radiates at −35° azimuth (starboard side) and 41.3 in. in front of the inlet. This corresponds to a polar angle of 41° down from the axis of the inlet. Turning on the blowing, either shaped as shown in figure 23 or uniformly as shown in figure 24, does not eliminate the sound radiation into the zone below the scarf inlet. In fact, it moves the peak toward 0° azimuth and, in the case of uniform blowing, increases the sound level by 1 or 2 dB. Figure 24 shows a rectangle of very low radiated sound at 30° azimuth and 52.2 in. axial (34.6° polar). This corresponds to a microphone in the hoop array that failed temporarily at one axial station.

Figures 25 and 26 show the contours at 80-percent engine speed. When the air injection is turned off, the sound radiated into the zone below the inlet is characterized by two lobes, one at −15° azimuth and 32.6 in. axial (48° polar) and a larger lobe at 85° azimuth and 21.7 in. axial (58.9° polar) (see fig. 25). When the shaped blowing is activated, the sound level in these two lobes increases by 2 dB, and the peak of the lobe closer to the inlet axis moves toward the axis. This is shown in figure 26. No data were obtained at 80-percent speed with uniform blowing.

Figures 27 through 29 show the contours of SPL at 90-percent speed with blowing off, shaped blowing on, and uniform blowing on, respectively. When the engine speed goes from 80 to 90 percent, the lobe of radiated sound that was directed off to the port side now moves inward to 60° azimuth, while the lobe at −15° azimuth moves to 0°. Turning the blowing on, whether uniform or shaped, intensifies these two lobes and also causes generation of a third lobe between these two at 32° azimuth.

It was not possible to gather reliable sound data at 100-percent speed because of the variability of engine speed at this setting due to inflow distortion.

The radiated sound level was evaluated at the frequency corresponding to twice BPF and contours were prepared. The data with the tubes in place at 0.125 in. from the highlight, but without any blowing on, are shown in figures 30 through 32 for engine speeds of 70, 80, and 90 percent, respectively. The ability of the scarf to redirect sound is not as clearly visible at twice BPF as it is at BPF. The difference between the sound level directly below the inlet and directly above is 3 dB or less. There is an indication of multiple lobes at 30.4 in. axial (polar angle 49.8°) on the port side of the inlet and at 21.7 in. axial (58.9°) on the starboard side at 70-percent speed, as seen in figure 30. An interesting feature at the two higher speeds, shown in figures 31 and 32, is that the lobes of higher sound level project farther upstream directly under the inlet and tend toward downstream azimuthally above the inlet. The effect is not symmetric; it tends to favor the port side of the inlet.

Figures 33 through 35 are the contours of BPF tone radiated from the scarf inlet with the air injection tubes removed and the inflow control device installed. The plots record directivity of the tone at 70-, 80-, and 90-percent fan speed, respectively. The contours are similar to those with the air injection tubes in

place (figs. 22 at 70 percent, 25 at 80 percent, and 27 at 90 percent), but the peak levels are 3 to 4 dB lower. The sound energy appears to be more uniformly distributed around the inlet with the inflow control device in place. Thus, it is more difficult to see the scarf noise reduction. While the sound level above the inlet is generally higher than anywhere else around the inlet, the shadow region below the inlet is not as clear. The inflow control device appears to reduce the amplitude of the turbulence ingestion, thereby reducing the turbulence-induced noise, more efficiently than any air injection configuration.

Figures 36 through 38 are contours of 1st harmonic of the BPF tone radiated from the scarf inlet with the air injection tubes removed and the inflow control device installed. The plots record directivity of the tone at 70-, 80-, and 90-percent fan speed, respectively. The sound level is less than the sound level measured with the air injection tubes in place and without the inflow control device. The peak sound level at BPF is 5 dB or more greater than the peak at 2 BPF for any engine speed. This is not an expected result because the model has been configured in such a way that the tone at BPF should not propagate, but the tone at twice BPF should.

Discussion of Results

Inlet blowing does not produce the inflow uniformity required to eliminate noise-producing inflow distortion. This is felt to be due to a lack of authority that arises from the design of the blowing hardware. The diameter of individual injection tubes is too small and flow in the tubes chokes, limiting the flow rate that the system is capable of producing. The presence of air injection tubes has a beneficial effect on reducing inflow distortion. It is postulated that the tubes perform as microvortex generators and reduce the acceleration of flow around the inlet lip on the crown half of the inlet by generating vortices in the flow stream.

Whereas the results indicate that the scarf inlet does reduce some of the fan-radiated sound below the inlet, inflow distortion causes turbulence that is ingested, thereby producing noise. Noise is radiated into a single, broad lobe below and to the side of the inlet. The source of this noise is felt to be the interaction of the rotor with ingested turbulence that is concentrated at the crown of the inlet. Because the noise source is located near the wall of the inlet, noise is focused by the curvature of the wall to radiate predominantly downward. The source wanders in the area of the crown as the turbulence bubble vascillates, thus the radiation lobe peak varies azimuthally in angles around 0°.

Concluding Remarks

The purpose of the boundary layer control is to simulate forward flight in the scarf inlet. Forward flight is expected to produce a circumferentially uniform boundary layer into the fan rotor. Although the number of boundary layer measurement transducers is limited in this study, the data obtained indicate that the boundary layer into the rotor is not uniform and that blowing into the boundary layer does not materially remedy this lack of uniformity. It is felt that the problem with the blowing is the design and an air injection system that provides more uniform distribution and greater authority could perform as expected. It is interesting to note that the air injection tubes themselves act as microvortex generators to reduce inflow nonuniformity. The impact of the tubes is a function of proximity to the inlet lip. The closer they are to the lip, the greater the effect. The tubes as microvortex generators did not achieve the desired result of simulating forward flight; however, it is expected that properly designed microvortex generators could be more successful.

The effectiveness of the scarf inlet to redirect some of the radiated noise away from the ground is demonstrated in these tests; however, the acoustic performance of the inlet is degraded by strong tones generated at blade passage frequency and its first harmonic. Sound is generated by interaction of the ingested turbulence and the fan rotor, and the generated sound radiates to the far field. The attempt to reduce the nonuniform inflow by way of inlet blowing was not successful.

References

1. Abbott, J. M.; and Slater, J. W.: Computational Study of the Aerodynamic Performance of Three-Dimensional Subsonic Inlets. AIAA-2001-3886, July 2001.

2. Clark, L. R.; Thomas, R. H.; Dougherty, R. P.; Farassat, F.; and Gerhold, C. H.: Inlet Shape Effects on the Far-Field Sound of a Model Fan. AIAA-97-1589, May 1997.

3. Chestnutt, D., ed.: *Flight Effects of Fan Noise*. NASA CP-2242, 1982.

4. Gerhold, C. H.; Clark, L. R.; and Biedron, R.: Control of Inflow Distortion in a Scarf Inlet. AIAA-2002-2432, June 2002.

5. Tyler, J. M.; and Sofrin, T. G.: Axial Flow Compressor Noise Studies. SAE Transactions, vol. 70, 1962, pp. 309–322.

6. Hodges, R. M.; Gerhold, C. H.; Balster, D.; and Thomas, R. H.: Acoustic Testing of Very High Bypass Ratio Turbofans Using Turbine Powered Scale Models. AIAA-94-2552, June 1994.

7. Thomas, R. H.; Farassat, F.; Clark, L. R.; and Gerhold, C. H.: Azimuthal Patterns of the Radiated Sound Field From a Turbofan Model. AIAA-97-1588, May 1997.

Table 1. Boundary Layer Thickness at Keel of Scarf Inlet on 12-in. ADP Demonstrator

Fan speed, percent	Ports at 0.125 in.			Ports at 0.500 in.			Ports at 0.875 in.			Unmodified	Wind tunnel M = 0.15
	No blowing	Uniform blowing	Shaped blowing	No blowing	Uniform blowing	Shaped blowing	No blowing	Uniform blowing	Shaped blowing		
70	0.123	0.127	0.130	0.114	0.113	0.115	0.119	0.124	0.125	0.129	0.086
80	.131	.135	.135	.121	.120	.122	.125	.129	.130	.136	
90	.142	.141	.142	.128	.126	.128	.132	.135	.134	.143	.095
100	.151	.150	.151	.135	.136	.138	.140	.142	.144	.210	.106

Table 2. Boundary Layer Thickness at Midpoint of Scarf Inlet on 12-in. ADP Demonstrator

Fan speed, percent	Ports at 0.125 in.			Ports at 0.500 in.			Ports at 0.875 in.			Unmodified	Wind tunnel M = 0.15
	No blowing	Uniform blowing	Shaped blowing	No blowing	Uniform blowing	Shaped blowing	No blowing	Uniform blowing	Shaped blowing		
70	0.150	0.152	0.127	0.153	0.197	0.172	0.171	0.297	0.157	0.298	0.059
80	.159	.158	.137	.168	.234	.189	.215	.306	.176	.318	
90	.170	.177	.162	.243	.280	.255	.268	.318	.267	.380	.095
100	.227	.257	.207	.303	.350	.301	.310	.396	.310	>.5	.097

Table 3. Calculated Inflow Mach Number to Rotor at Crown of Scarf Inlet on 12-in. ADP Demonstrator

Fan speed, percent	Ports at 0.125 in.			Ports at 0.500 in.			Ports at 0.875 in.			Unmodified	Wind tunnel M = 0.15
	No blowing	Uniform blowing	Shaped blowing	No blowing	Uniform blowing	Shaped blowing	No blowing	Uniform blowing	Shaped blowing		
70	0.437	0.449	0.454	0.422	0.431	0.459	0.438	0.423	0.423	0.447	0.351
80	.514	.522	.524	.503	.512	.528	.517	.503	.509	.521	
90	.596	.605	.606	.596	.596	.606	.601	.594	.601	.597	.473
100	.686	.684	.690	.680	.684	.686	.687	.686	.689	.653	.549

Table 4. Calculated Inflow Mach Number to Rotor at Midpoint of Scarf Inlet on 12-in. ADP Demonstrator

Fan speed, percent	Ports at 0.125 in.			Ports at 0.500 in.			Ports at 0.875 in.			Unmodified	Wind tunnel M = 0.15
	No blowing	Uniform blowing	Shaped blowing	No blowing	Uniform blowing	Shaped blowing	No blowing	Uniform blowing	Shaped blowing		
70	0.322	0.321	0.321	0.320	0.322	0.327	0.321	0.323	0.322	0.316	0.324
80	.376	.372	.371	.377	.377	.377	.376	.380	.379	.370	
90	.435	.434	.431	.438	.436	.433	.436	.440	.438	.426	.429
100	.506	.498	.497	.502	.505	.497	.501	.506	.502	.467	.494

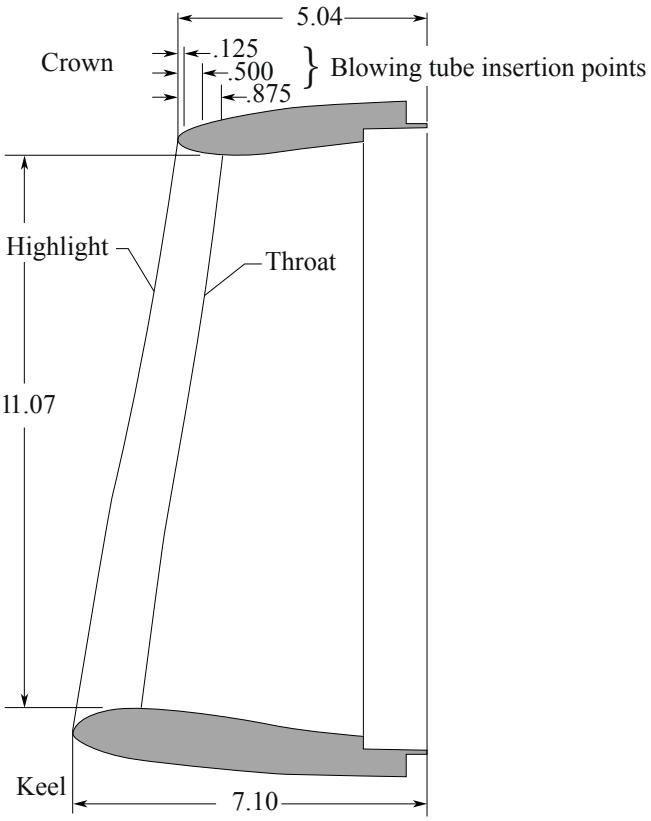

(a) Sketch indicating locations of terms used in report.

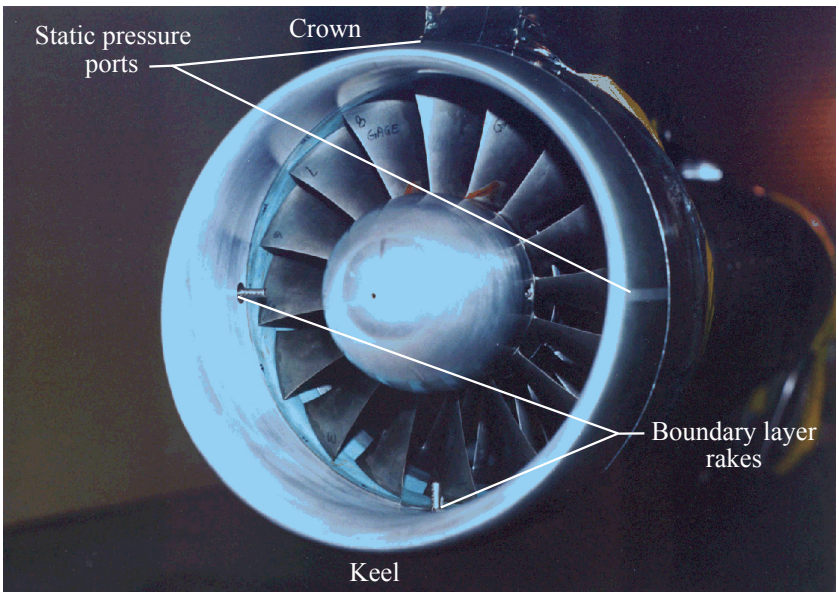

(b) Image of 12-in. ADP Demonstrator with scarf inlet showing boundary layer rakes in place in front of fan rotor.

Figure 1. Scarf inlet.

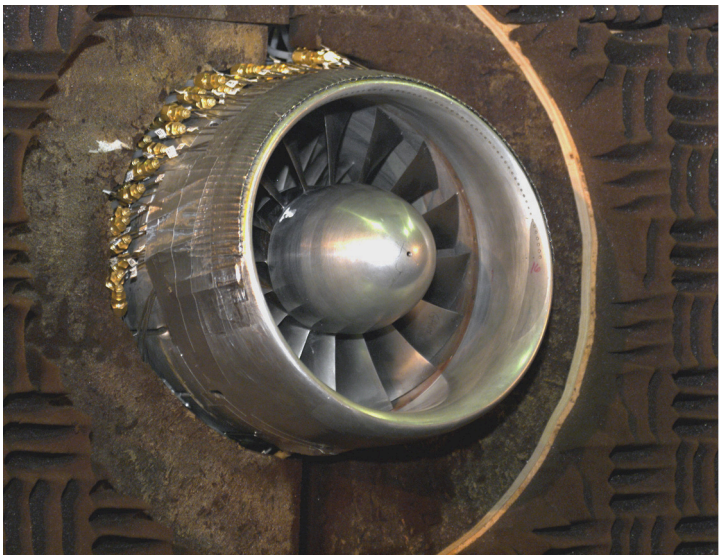

Figure 2. Closeup of 12-in. ADP Demonstrator scarf inlet with external blowing tubes attached at 0.125 in. from inlet highlight.

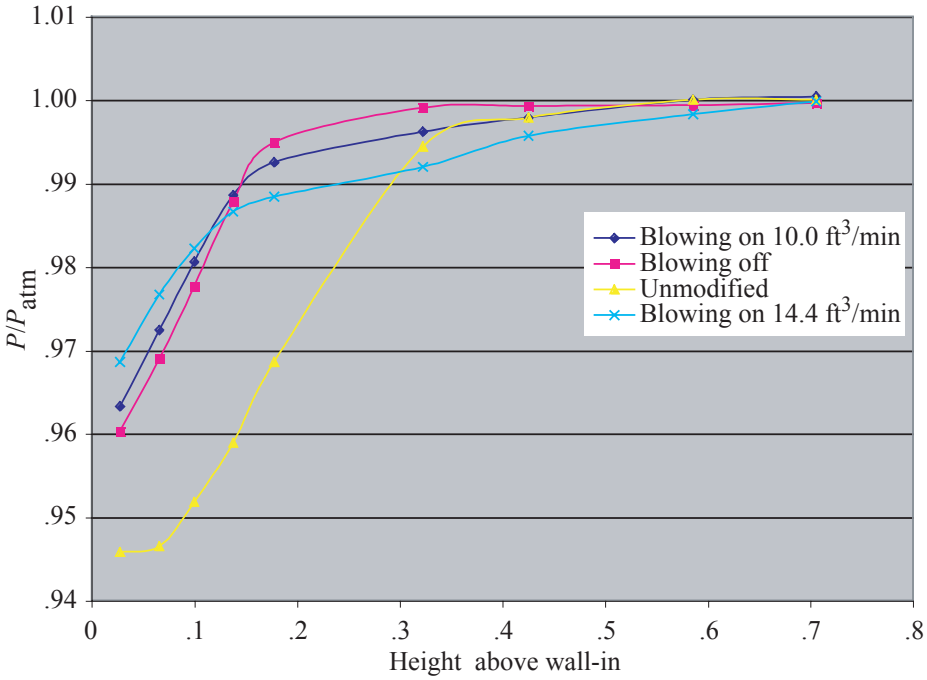

Figure 3. Boundary layer profile at midpoint at 70-percent speed, ports at 0.125 in., uniform blowing.

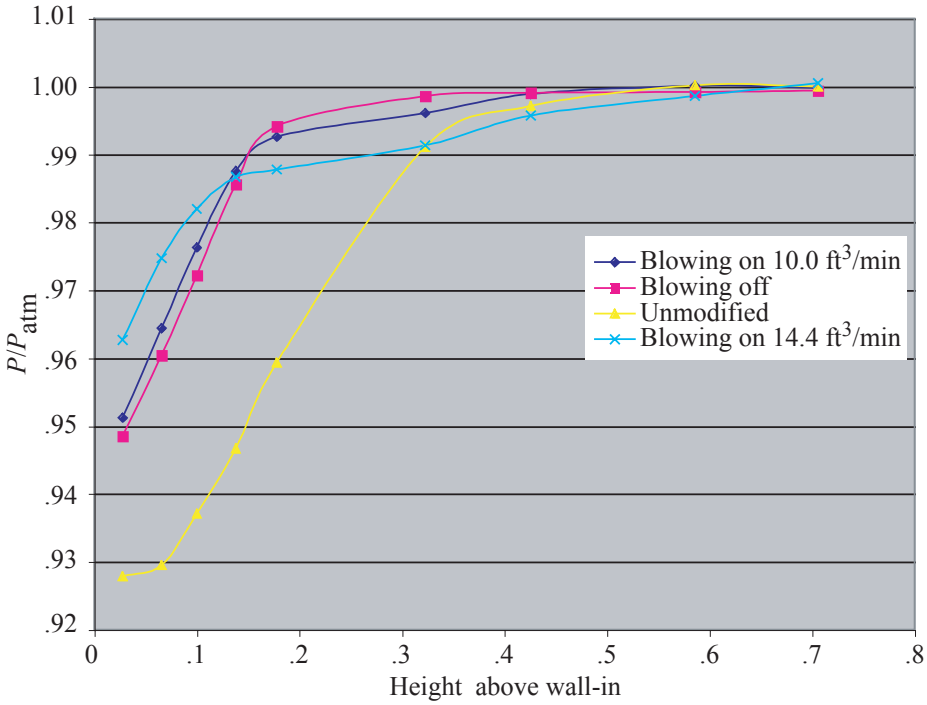

Figure 4. Boundary layer profile at midpoint at 80-percent speed, ports at 0.125 in., uniform blowing.

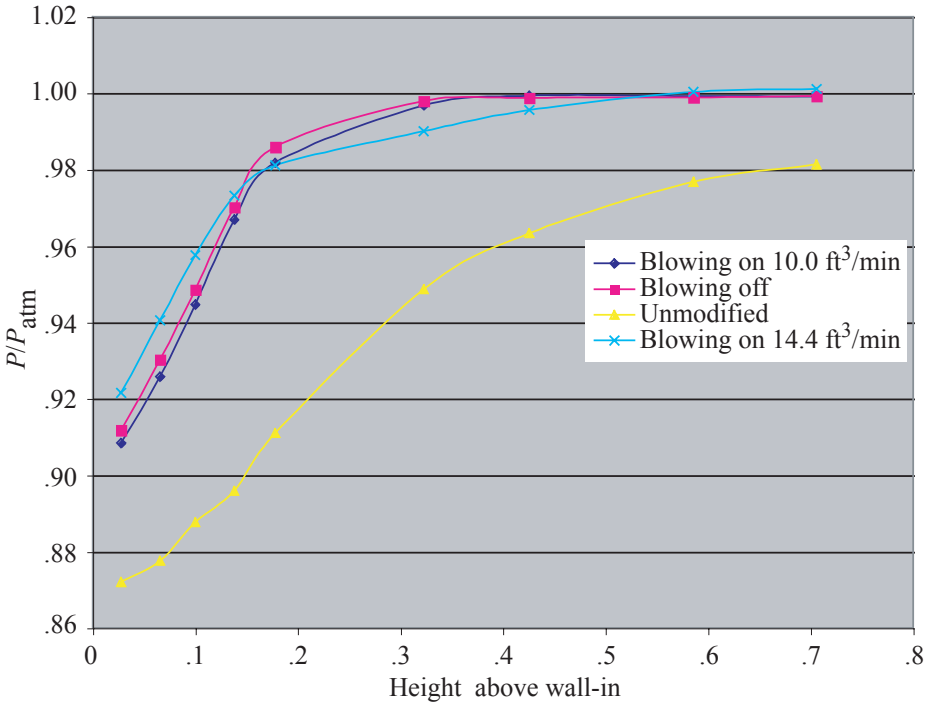

Figure 5. Boundary layer profile at midpoint at 100-percent speed, ports at 0.125 in., uniform blowing.

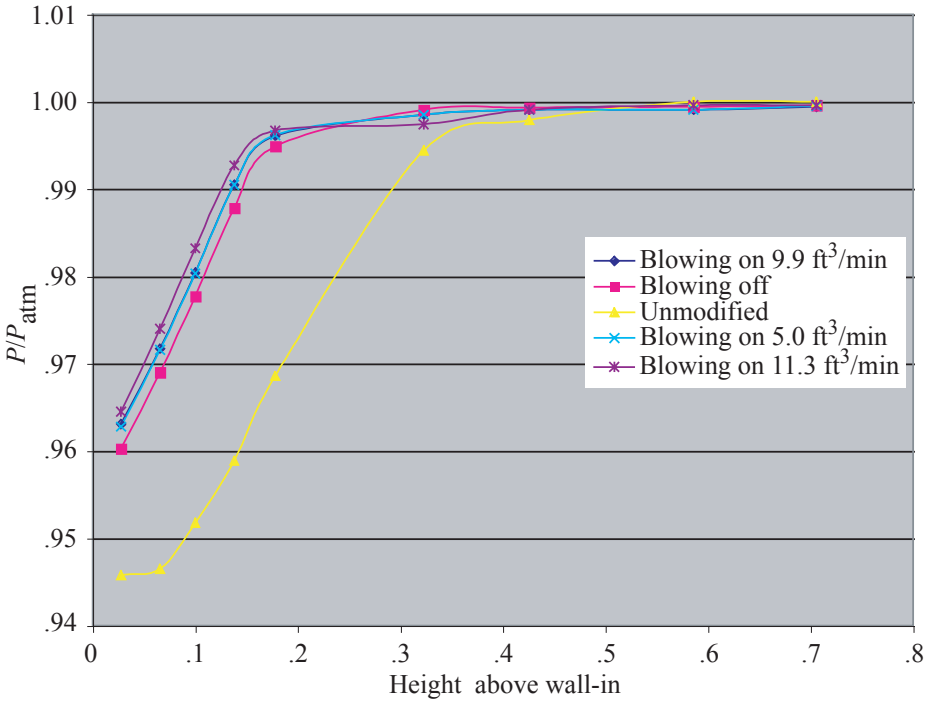

Figure 6. Boundary layer profile at midpoint at 70-percent speed, ports at 0.125 in., shaped blowing.

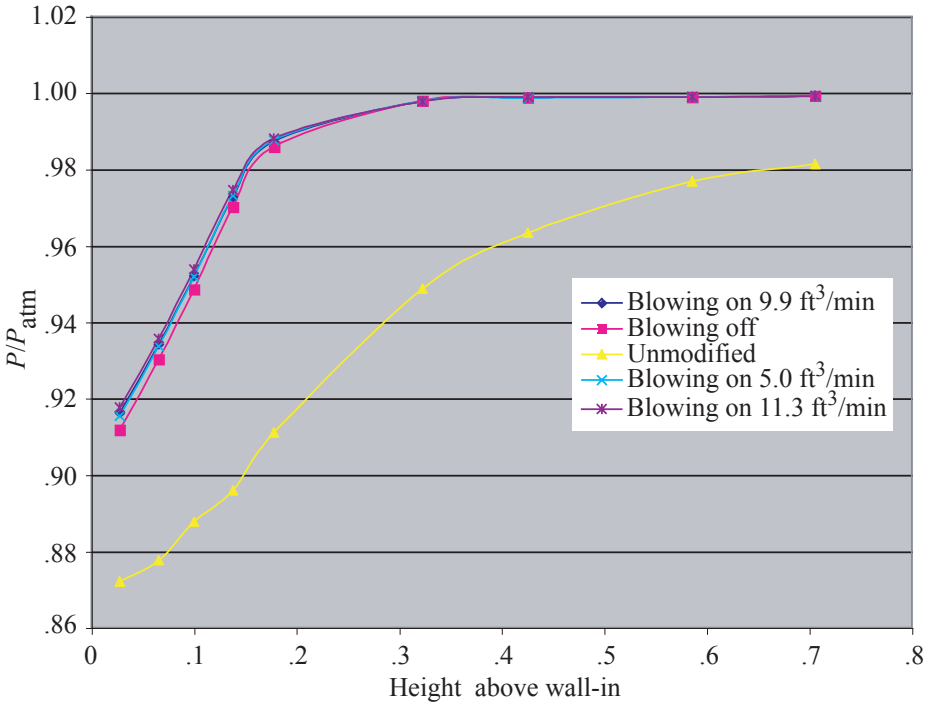

Figure 7. Boundary layer profile at midpoint at 100-percent speed, ports at 0.125 in., shaped blowing.

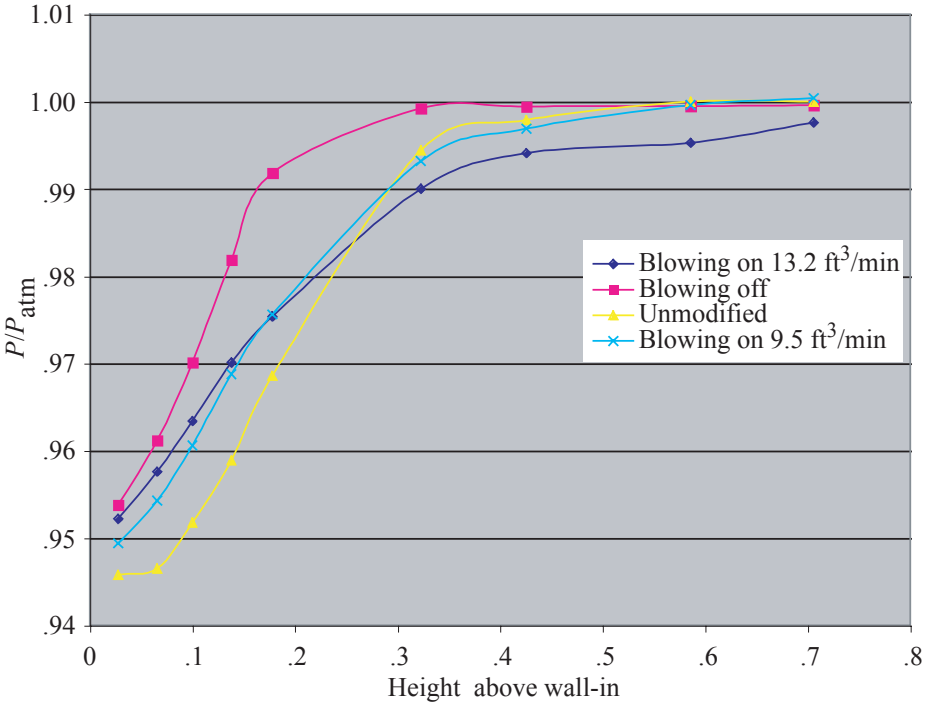

Figure 8. Boundary layer profile at midpoint at 70-percent speed, ports at 0.875 in., uniform blowing.

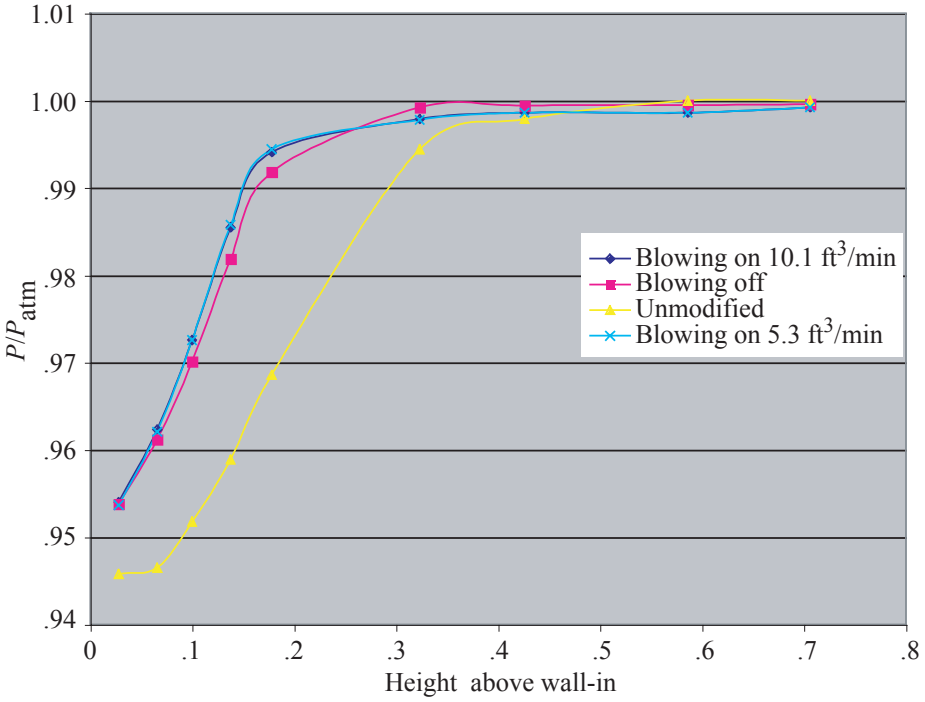

Figure 9. Boundary layer profile at midpoint at 70-percent speed, ports at 0.875 in., shaped blowing.

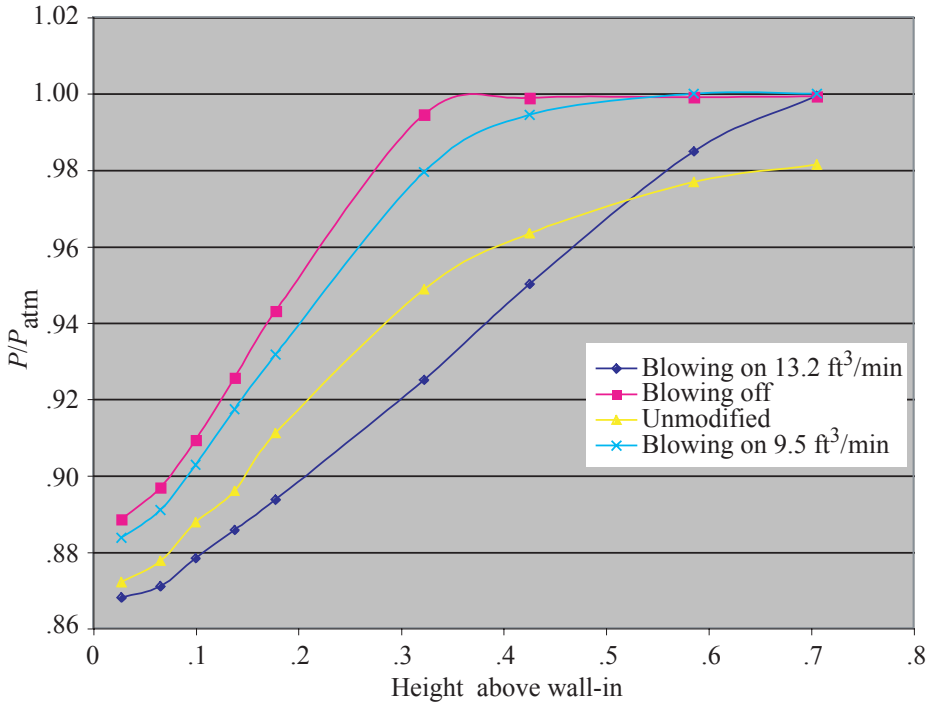

Figure 10. Boundary layer profile at midpoint at 100-percent speed, ports at 0.875 in., uniform blowing.

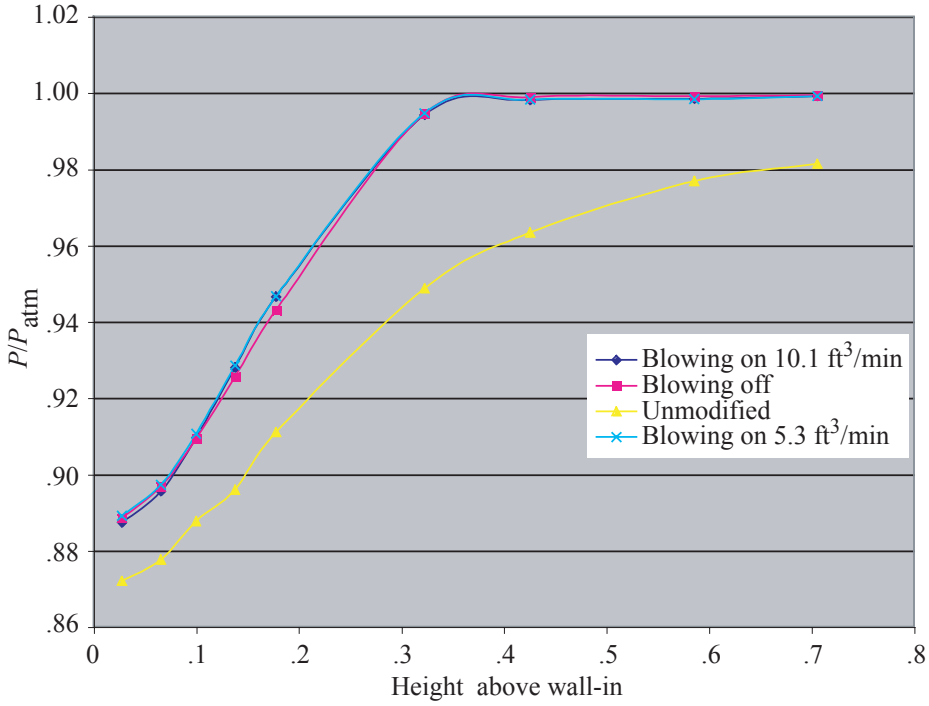

Figure 11. Boundary layer profile at midpoint at 100-percent speed, ports at 0.875 in., shaped blowing.

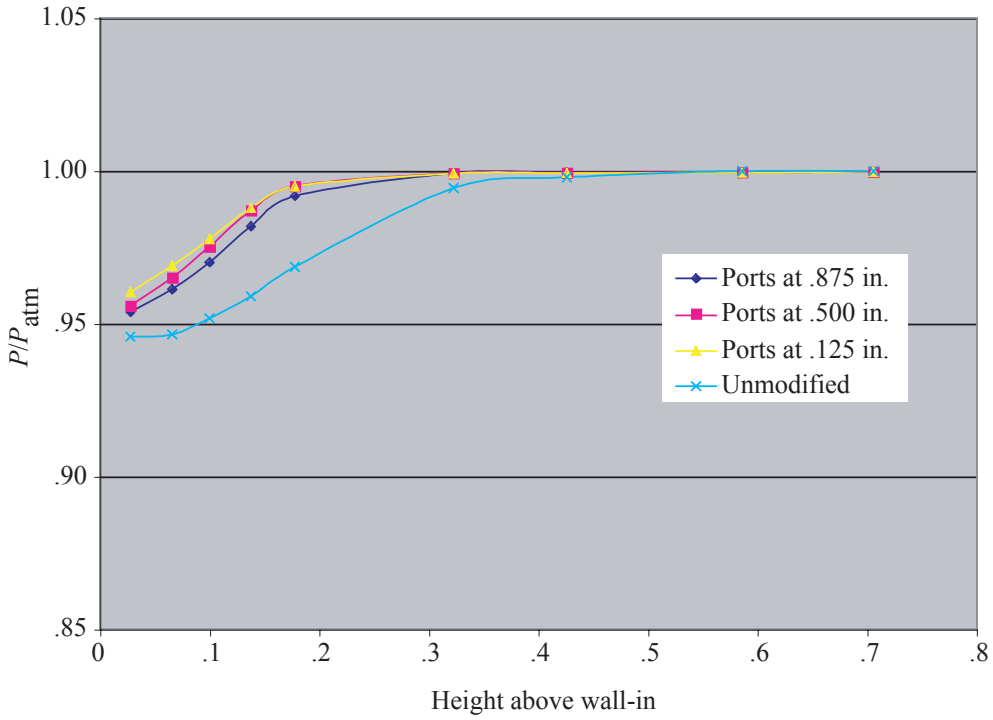

Figure 12. Effect of blowing tube placement (blowing off) on boundary layer profile at midpoint at 70-percent speed.

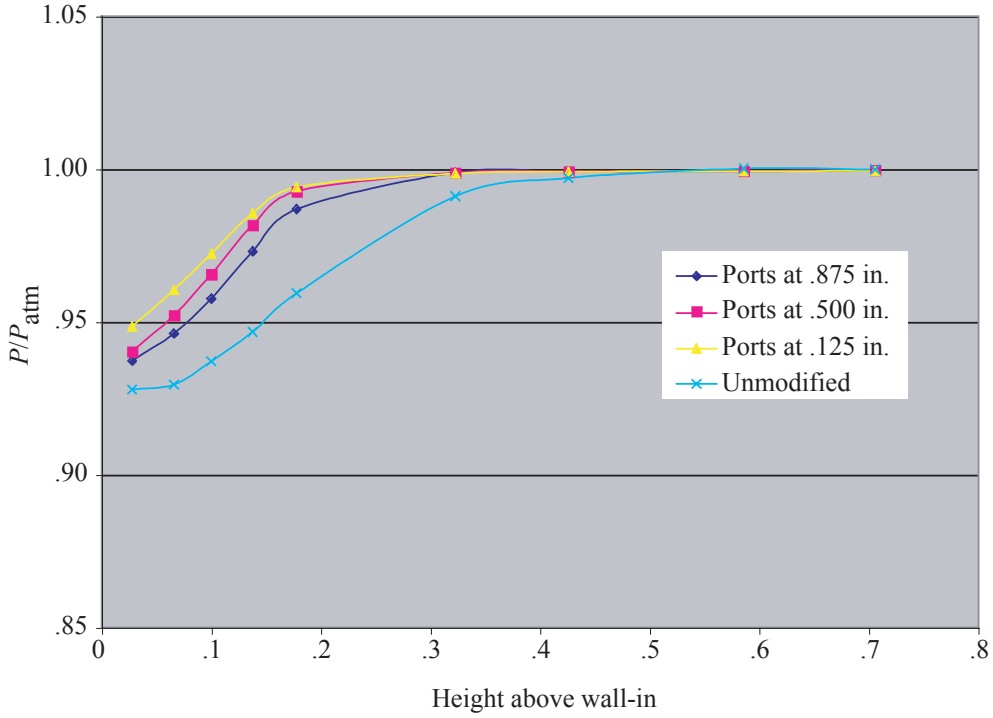

Figure 13. Effect of blowing tube placement (blowing off) on boundary layer profile at midpoint at 80-percent speed.

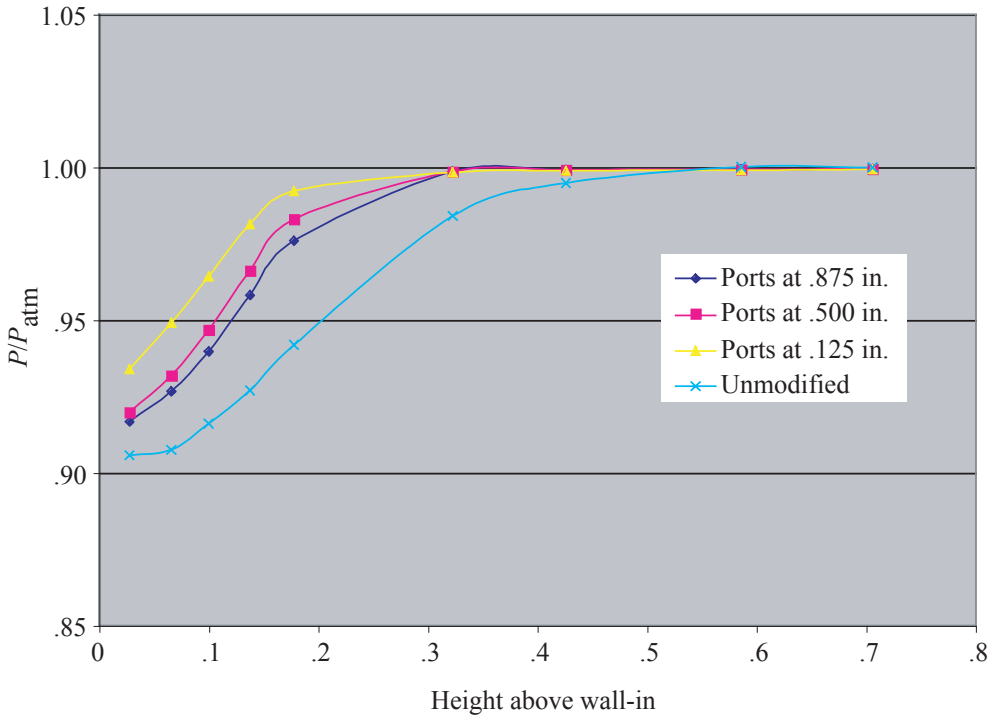

Figure 14. Effect of blowing tube placement (blowing off) on boundary layer profile at midpoint at 90-percent speed.

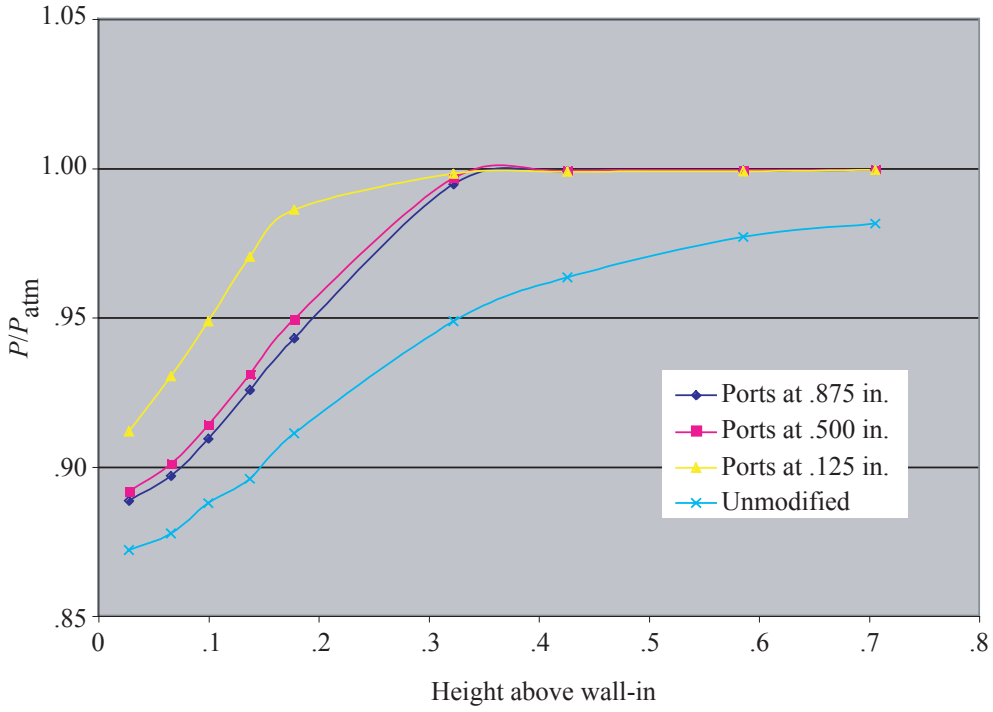

Figure 15. Effect of blowing tube placement (blowing off) on boundary layer profile at midpoint at 100-percent speed.

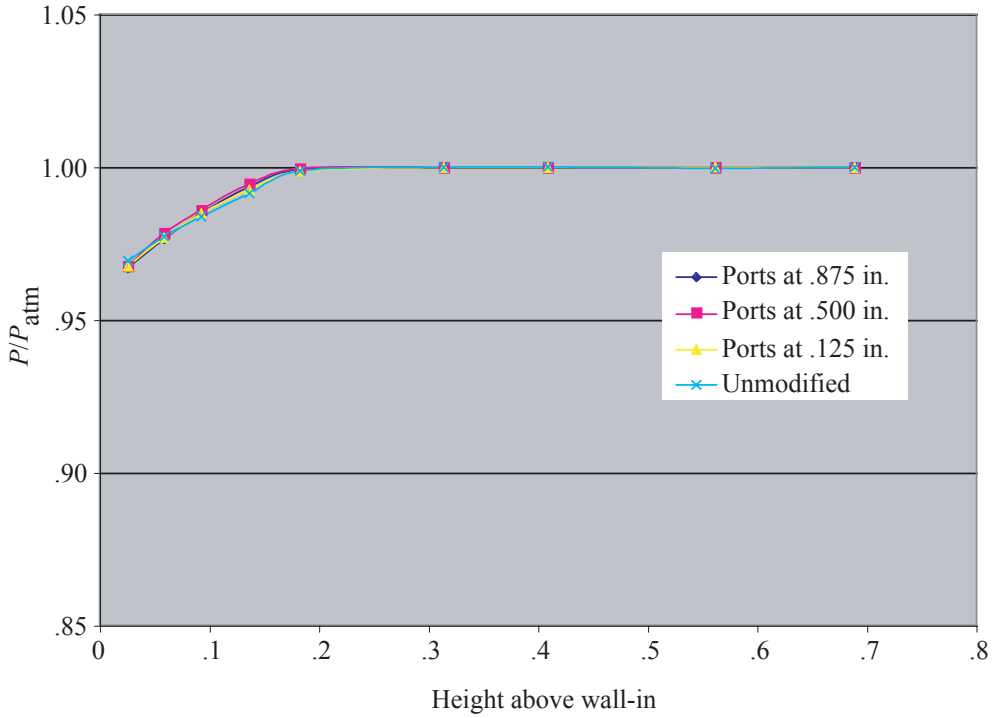

Figure 16. Effect of blowing tube placement (blowing off) on boundary layer profile on keel at 70-percent speed.

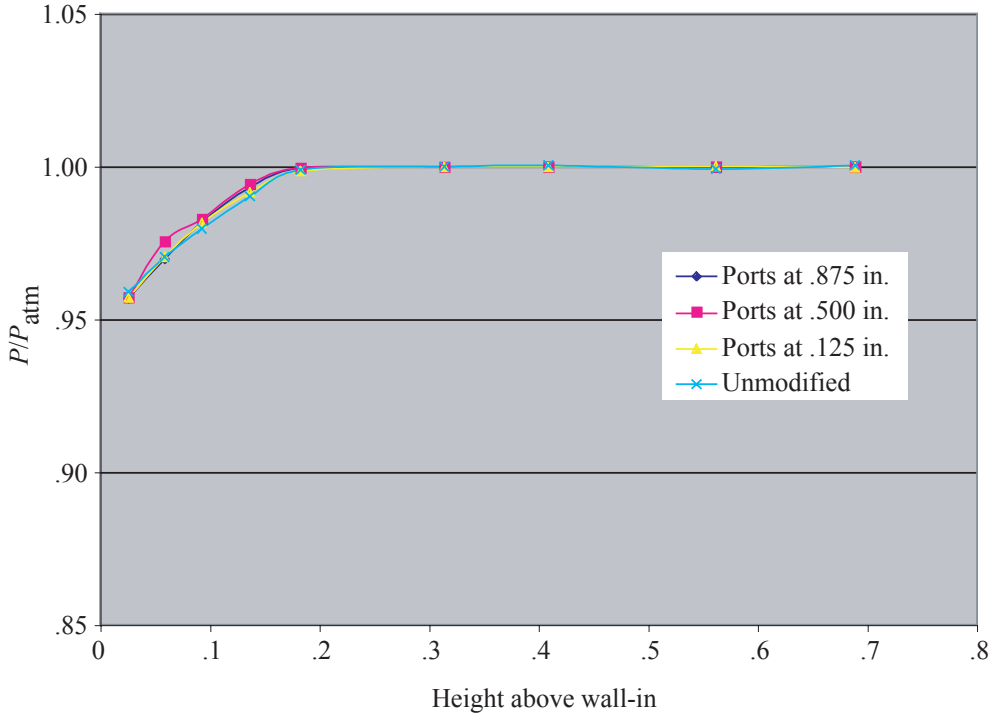

Figure 17. Effect of blowing tube placement (blowing off) on boundary layer profile on keel at 80-percent speed.

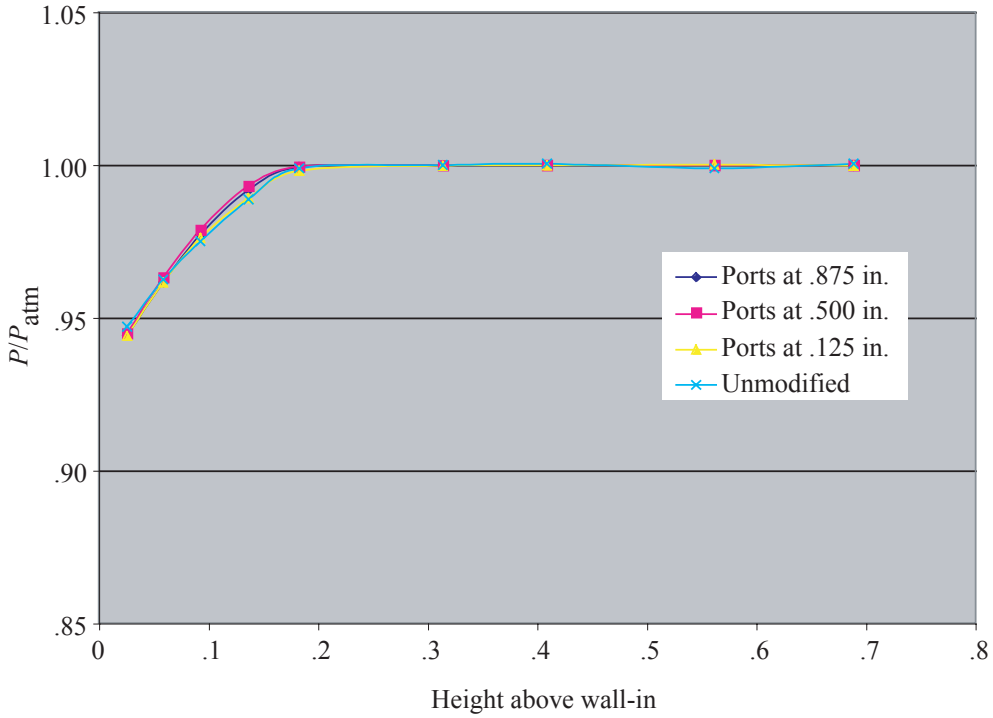

Figure 18. Effect of blowing tube placement (blowing off) on boundary layer profile on keel at 90-percent speed.

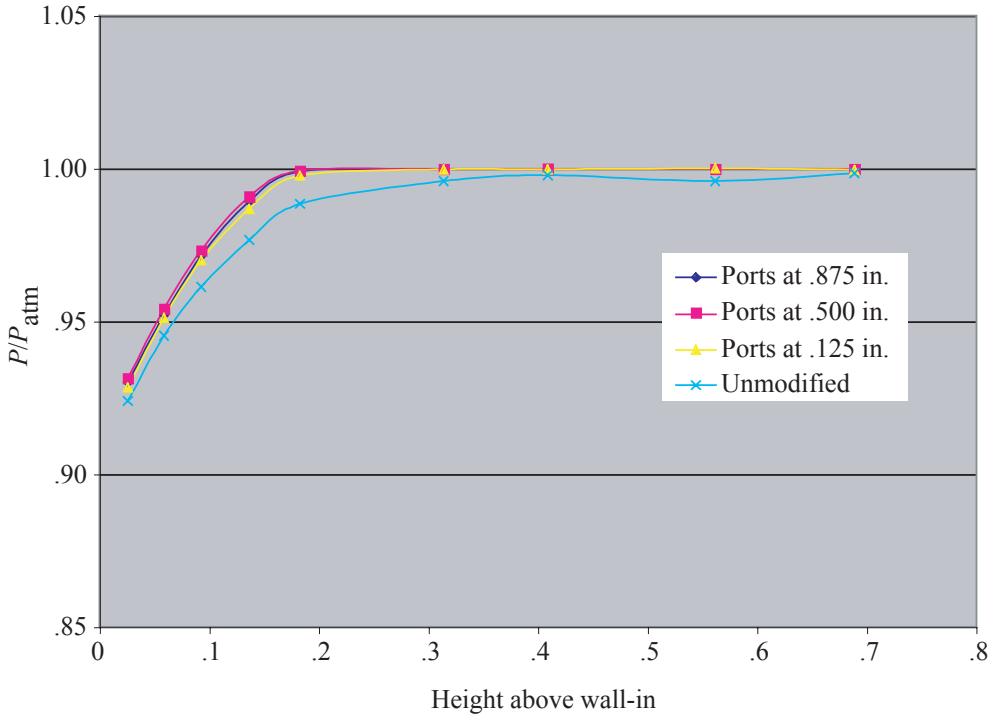

Figure 19. Effect of blowing tube placement (blowing off) on boundary layer profile on keel at 100-percent speed.

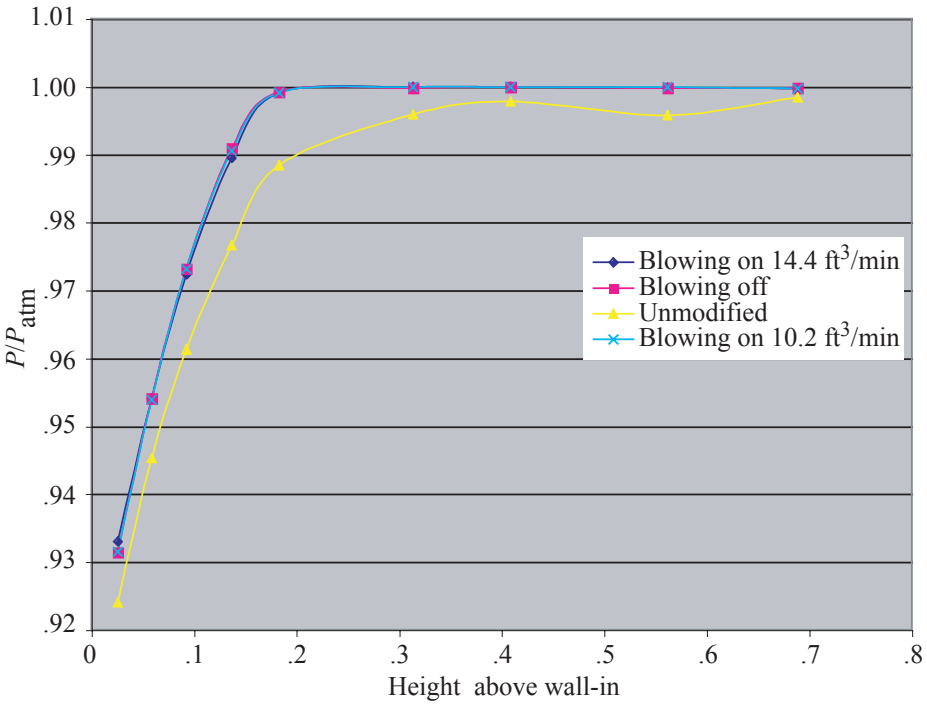

Figure 20. Boundary layer profile on keel at 100-percent speed, ports at 0.50 in., uniform blowing.

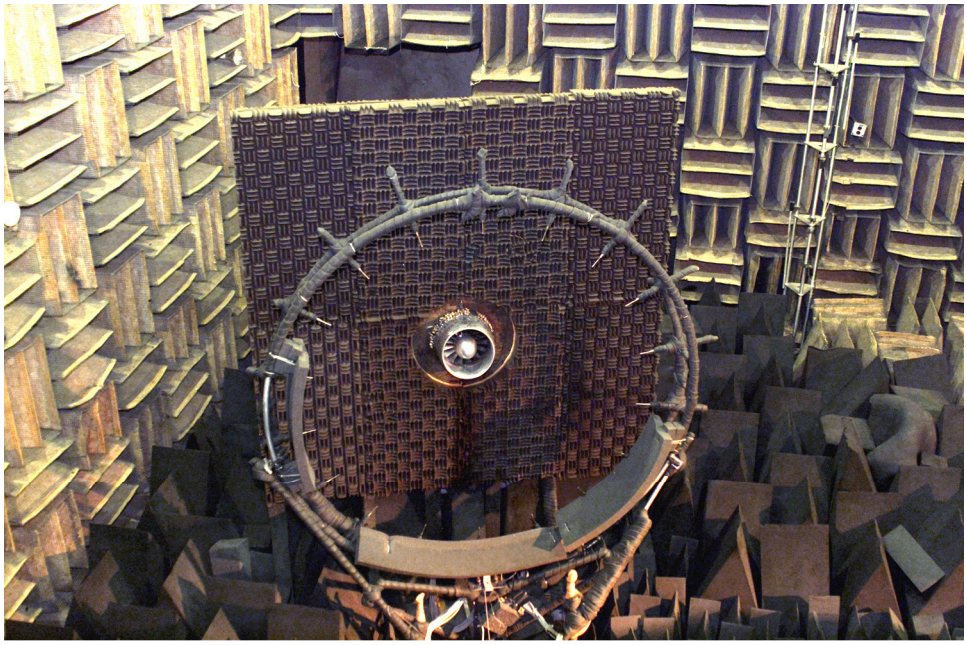

Figure 21. Image of 12-in. ADP Demonstrator with scarf inlet, configured for inlet boundary layer control by blowing, in the anechoic chamber. Figure also shows microphone hoop array.

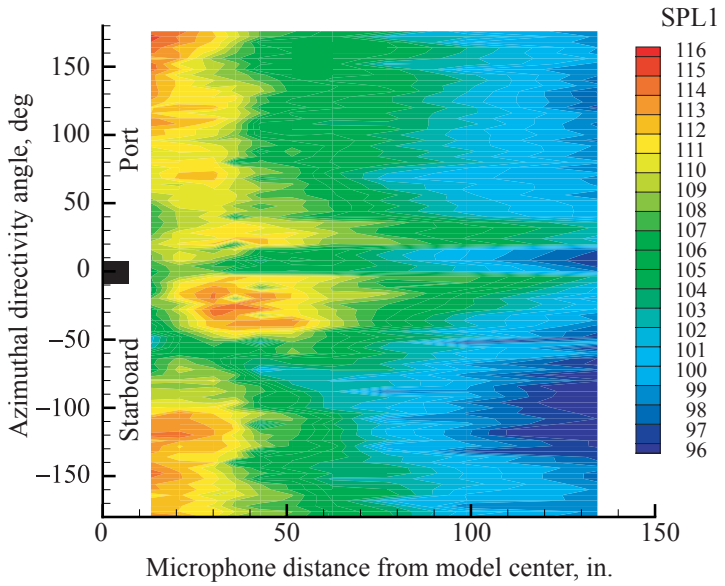

Figure 22. Contour of BPF tone, 70-percent fan speed, air injection tubes at 0.125 in. from highlight, air flow off.

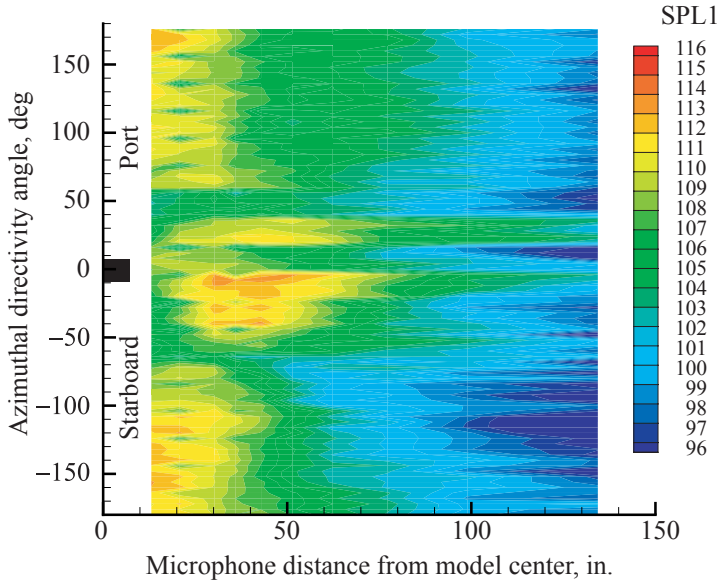

Figure 23. Contour of BPF tone, 70-percent speed, air injection tubes at 0.125 in. from highlight, air flow on shaped blowing.

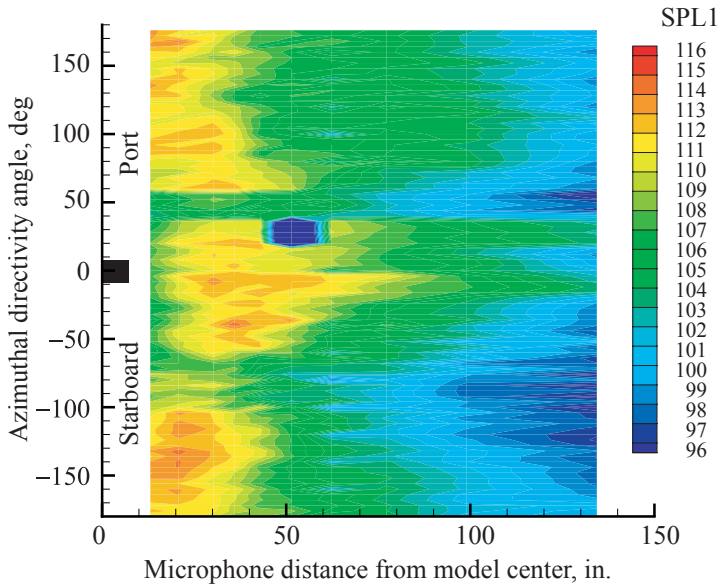

Figure 24. Contour of BPF tone, 70-percent speed, air injection tubes at 0.125 in. from highlight, air flow on uniform blowing.

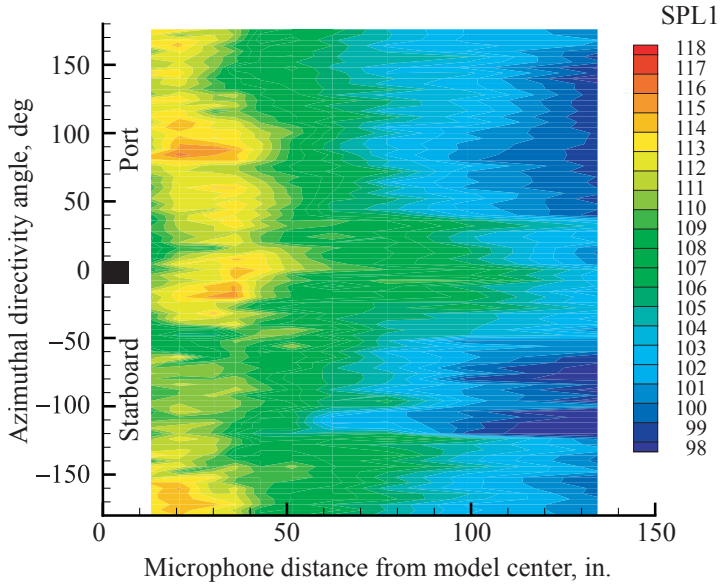

Figure 25. Contour of BPF tone, 80-percent speed, air injection tubes at 0.125 in. from highlight, air flow off.

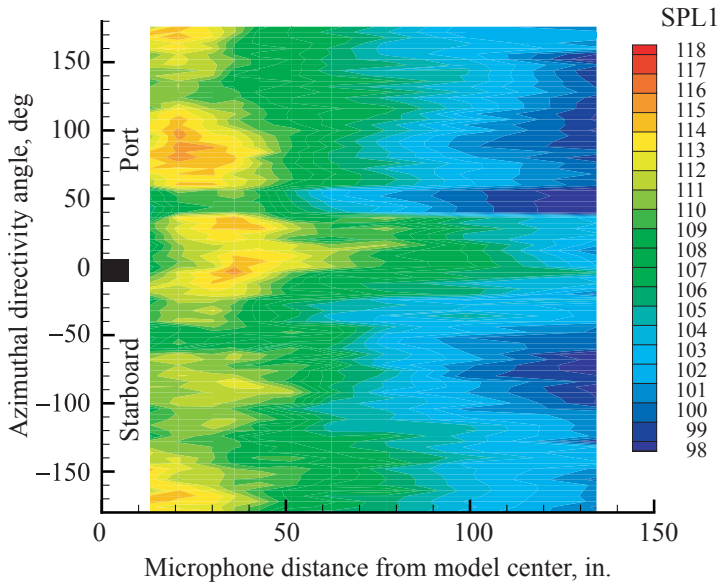

Figure 26. Contour of BPF tone, 80-percent speed, air injection tubes at 0.125 in. from highlight, air flow on shaped blowing.

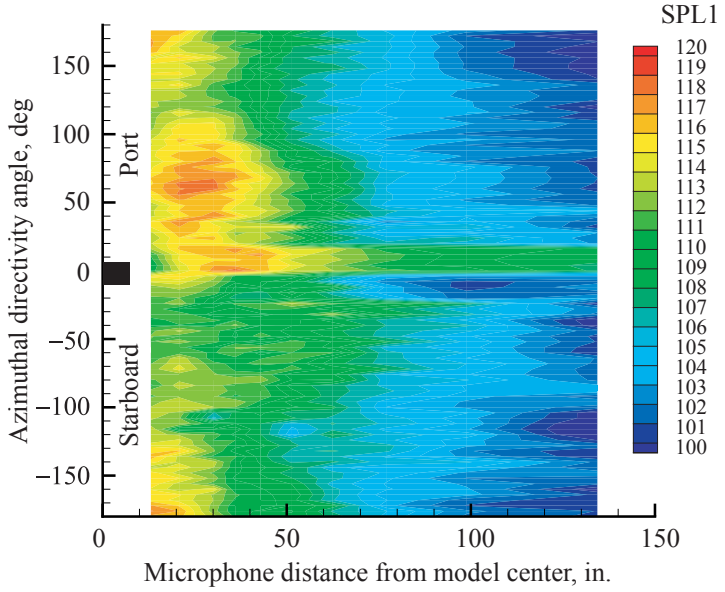

Figure 27. Contour of BPF tone, 90-percent speed, air injection tubes at 0.125 in. from highlight, air flow off.

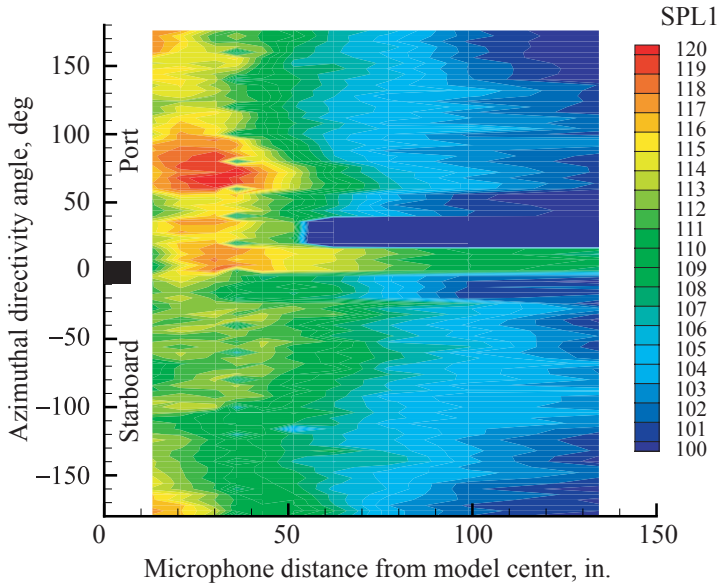

Figure 28. Contour of BPF tone, 90-percent speed, air injection tubes at 0.125 in. from highlight, air flow on shaped blowing.

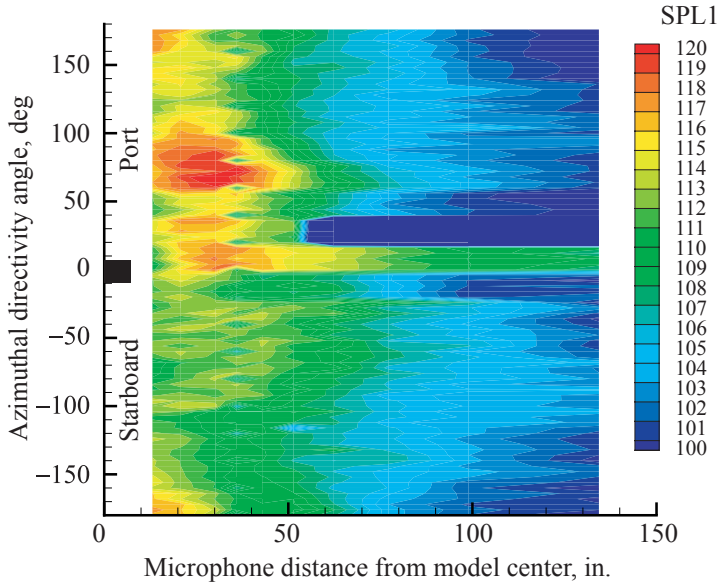

Figure 29. Contour of BPF tone, 90-percent speed, air injection tubes at 0.125 in. from highlight, air flow on uniform blowing.

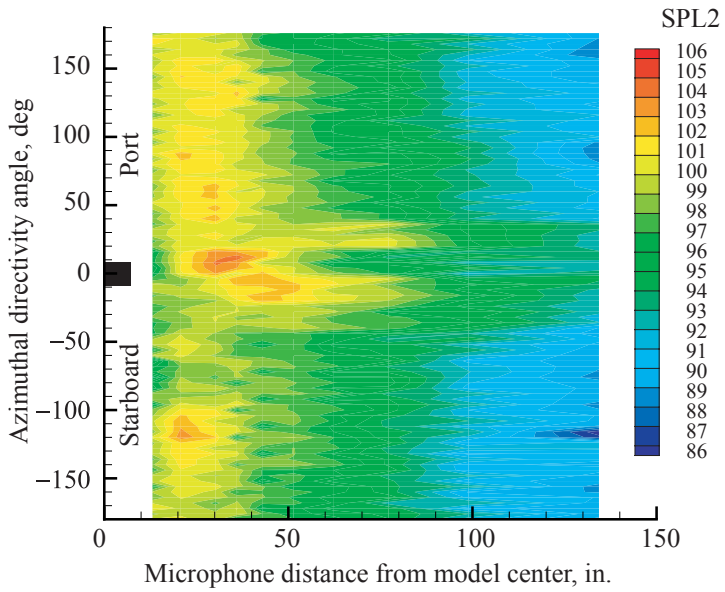

Figure 30. Contour of 2 × BPF tone, 70-percent speed, air injection tubes at 0.125 in. from highlight, air flow off.

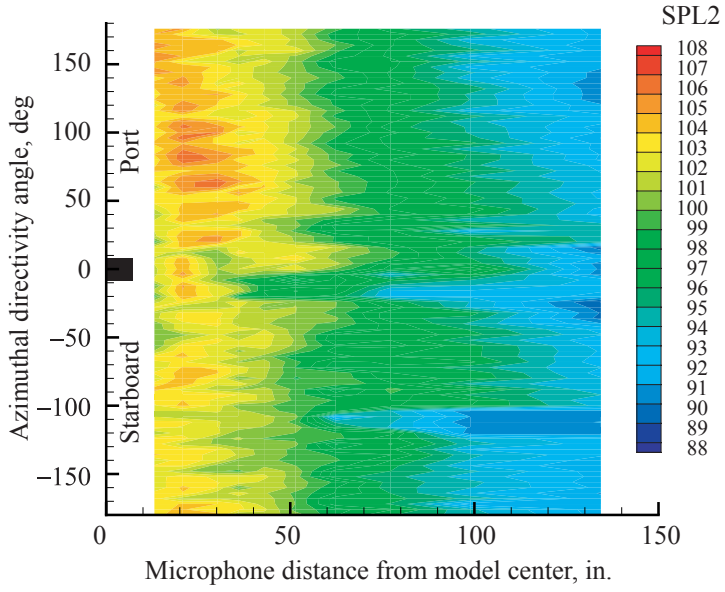

Figure 31. Contour of 2 × BPF tone, 80-percent speed, air injection tubes at 0.125 in. from highlight, air flow off.

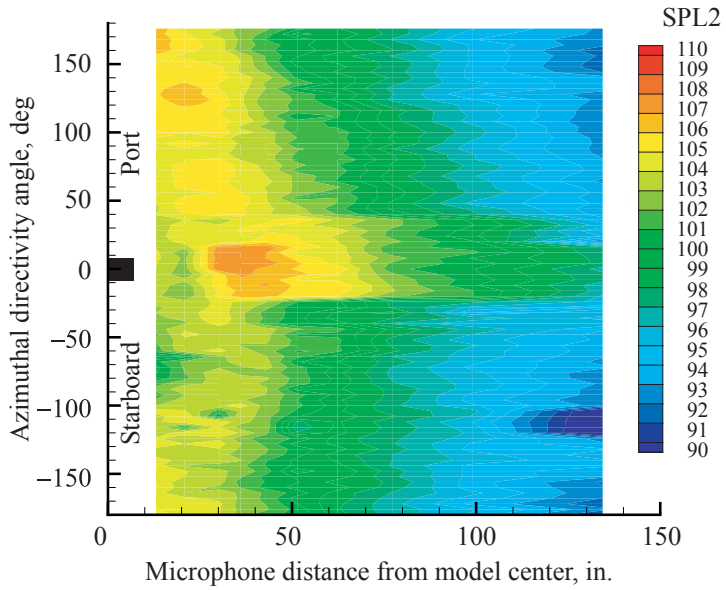

Figure 32. Contour of 2 × BPF tone, 90-percent speed, air injection tubes at 0.125 in. from highlight, air flow off.

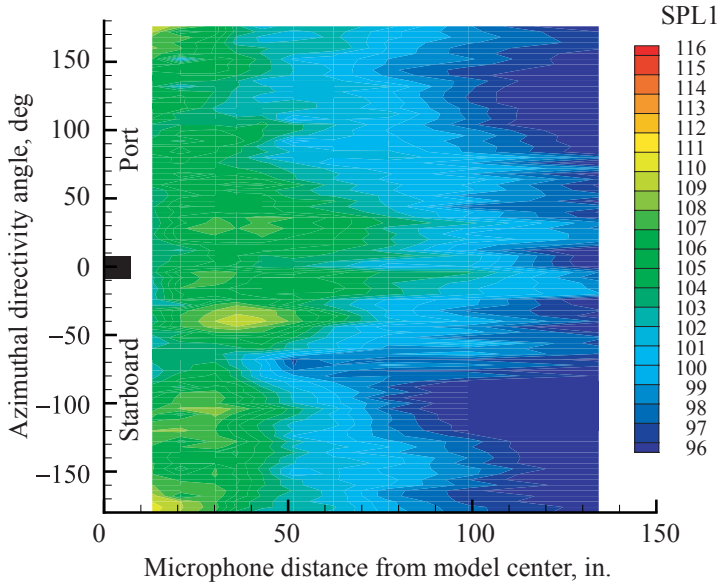

Figure 33. Contour of BPF tone, 70-percent speed, air injection tubes removed, ICD installed.

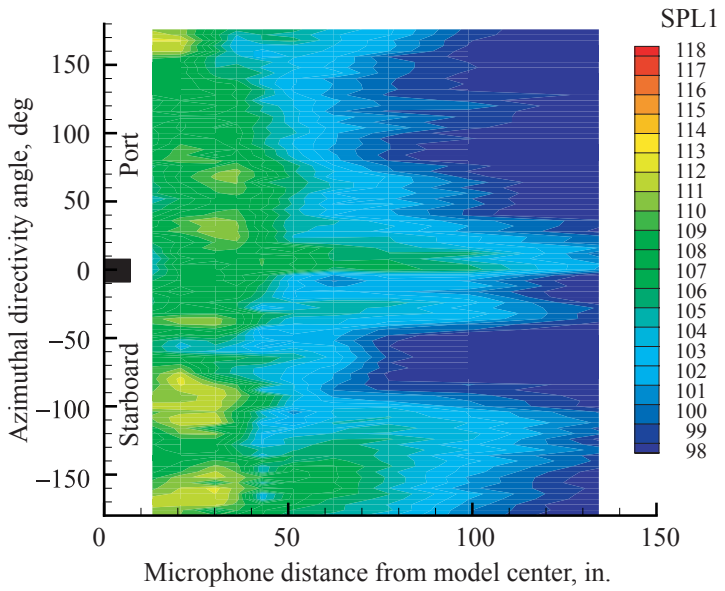

Figure 34. Contour of BPF tone, 80-percent speed, air injection tubes removed, ICD installed.

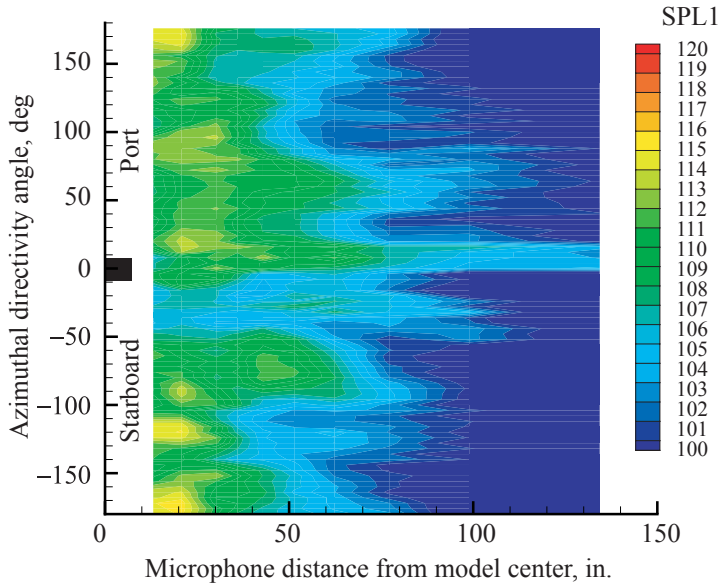

Figure 35. Contour of BPF tone, 90-percent speed, air injection tubes removed, ICD installed.

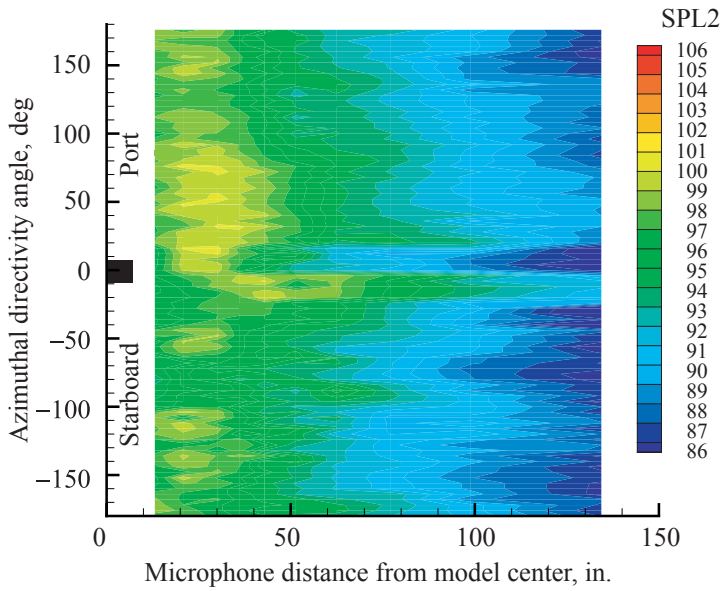

Figure 36. Contour of 2 × BPF tone, 70-percent speed, air injection tubes removed, ICD installed.

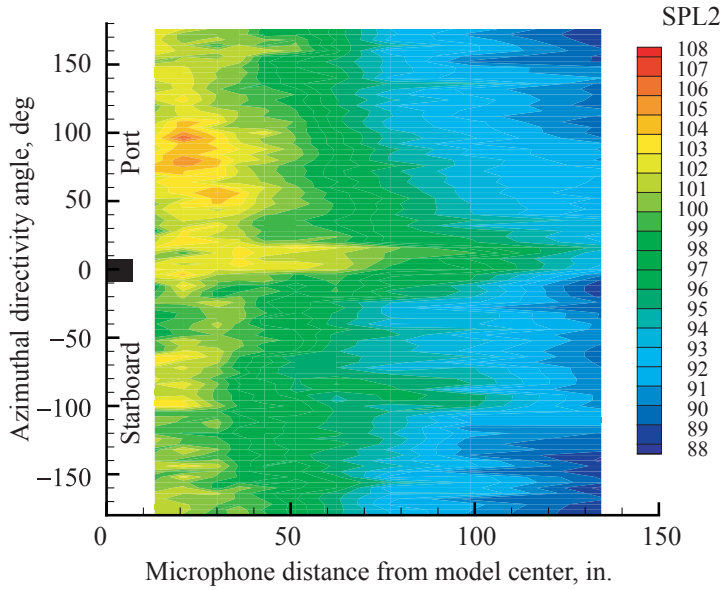

Figure 37. Contour of 2 × BPF tone, 80-percent speed, air injection tubes removed, ICD installed.

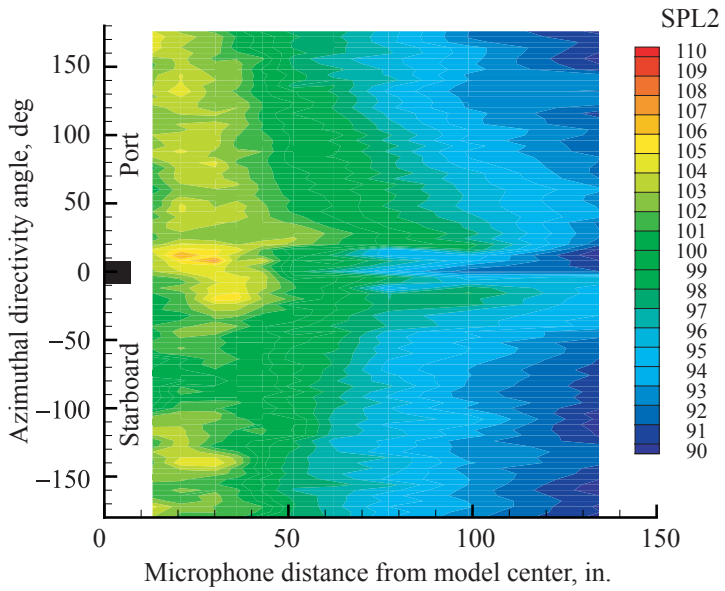

Figure 38. Contour of 2 × BPF tone, 90-percent speed, air injection tubes removed, ICD installed.

REPORT DOCUMENTATION PAGE

Form Approved
OMB No. 0704-0188

1. REPORT DATE *(DD-MM-YYYY)*	2. REPORT TYPE	3. DATES COVERED *(From - To)*
01- 12 - 2004	Technical Memorandum	

4. TITLE AND SUBTITLE
Effect of Blowing on Boundary Layer of Scarf Inlet

5a. CONTRACT NUMBER

5b. GRANT NUMBER

5c. PROGRAM ELEMENT NUMBER

6. AUTHOR(S)
Gerhold, Carl H.; and Clark, Lorenzo R.

5d. PROJECT NUMBER

5e. TASK NUMBER

5f. WORK UNIT NUMBER
781-30-14-01

7. PERFORMING ORGANIZATION NAME(S) AND ADDRESS(ES)
NASA Langley Research Center
Hampton, VA 23681-2199

8. PERFORMING ORGANIZATION REPORT NUMBER
L-18369

9. SPONSORING/MONITORING AGENCY NAME(S) AND ADDRESS(ES)
National Aeronautics and Space Administration
Washington, DC 20546-0001

10. SPONSOR/MONITOR'S ACRONYM(S)
NASA

11. SPONSOR/MONITOR'S REPORT NUMBER(S)
NASA/TM-2004-213267

12. DISTRIBUTION/AVAILABILITY STATEMENT
Unclassified - Unlimited
Subject Category 71
Availability: NASA CASI (301) 621-0390

13. SUPPLEMENTARY NOTES
Gerhold and Clark, Langley Research Center.
An electronic version can be found at http://ntrs.nasa.gov

14. ABSTRACT

When aircraft operate in stationary or low speed conditions, airflow into the engine accelerates around the inlet lip and pockets of turbulence that cause noise and vibration can be ingested. This problem has been encountered with engines equipped with the scarf inlet, both in full scale and in model tests, where the noise produced during the static test makes it difficult to assess the noise reduction performance of the scarf inlet. NASA Langley researchers have implemented boundary layer control in an attempt to reduce the influence of the flow nonuniformity in a 12-in. diameter model of a high bypass fan engine mounted in an anechoic chamber. Static pressures and boundary layer profiles were measured in the inlet and far field acoustic measurements were made to assess the effectiveness of the blowing treatment. The blowing system was found to lack the authority to overcome the inlet distortions. Methods to improve the implementation of boundary layer control to reduce inlet distortion are discussed.

15. SUBJECT TERMS
Inlet noise control; Boundary layer control; Inlet airflow distortion

16. SECURITY CLASSIFICATION OF:			17. LIMITATION OF ABSTRACT	18. NUMBER OF PAGES	19a. NAME OF RESPONSIBLE PERSON
a. REPORT	b. ABSTRACT	c. THIS PAGE			STI Help Desk (email: help@sti.nasa.gov)
					19b. TELEPHONE NUMBER *(Include area code)*
U	U	U	UU	35	(301) 621-0390